

Star formation, starbursts and quenching across the Coma supercluster

Smriti Mahajan^{*}, Chris P. Haines, Somak Raychaudhury

School of Physics and Astronomy, University of Birmingham, Birmingham B15 2TT, UK

ABSTRACT

We analyse Spitzer MIPS $24\mu\text{m}$ observations, and Sloan Digital Sky Survey (DR7) optical broadband photometry and spectra, to investigate the star formation properties of galaxies residing in the Coma supercluster region. We find that star formation (SF) in dwarf galaxies is quenched only in the high density environment at the centre of clusters and groups, but that passively-evolving massive galaxies are found in all environments, indicating that massive galaxies can become passive via internal processes. The SF-density relation observed for the massive galaxies is weaker relative to the dwarfs, but both show a trend for the fraction of star-forming galaxies (f_{SF}) declining to ~ 0 in the cluster cores. We find AGN activity is also suppressed among massive galaxies residing in the cluster cores.

We present evidence for a strong dependence of the mechanism(s) responsible for quenching star formation in dwarf galaxies on the cluster potential, resulting in two distinct evolutionary pathways. Firstly, we find a significant increase (at the 3σ level) in the mean equivalent width of $\text{H}\alpha$ emission among star-forming dwarf galaxies in the infall regions of the Coma cluster and the core of Abell 1367 with respect to the overall supercluster population, indicative of the infalling dwarf galaxies undergoing a starburst phase. We identify these starburst galaxies as the precursors of the post-starburst k+A galaxies. Extending the survey of k+A galaxies over the whole supercluster region, we find 11.4% of all dwarf ($z \text{ mag} > 15$) galaxies in the Coma cluster and 4.8% in the Abell 1367 have post-starburst like spectra, while this fraction is just 2.1% when averaged over the entire supercluster region (excluding the clusters). This points to a cluster-specific evolutionary process in which infalling dwarf galaxies undergo a starburst and subsequent rapid quenching due to their passage through the dense ICM. In galaxy groups, the star formation in infalling dwarf galaxies is instead slowly quenched due to the reduced efficiency of ram-pressure stripping.

We show that in the central $\sim 2 h_{70}^{-1}$ Mpc of the Coma cluster, the $(24-z)$ near/mid infrared colour of galaxies is correlated with their optical $(g-r)$ colour and $\text{H}\alpha$ emission, separating all mid-infrared (MIR) detected galaxies into two distinct classes of ‘red’ and ‘blue’. By analysing the spatial and velocity distribution of galaxies detected at $24\mu\text{m}$ in Coma, we find that the (optically) red $24\mu\text{m}$ detected galaxies follow the general distribution of ‘all’ the spectroscopic members, but their (optically) blue counterparts (i) are almost completely absent in the central $\sim 0.5 h_{70}^{-1}$ Mpc of Coma, and (ii) have a remarkable peak in their velocity distribution, corresponding to the mean radial velocity of the galaxy group NGC 4839, suggesting that a significant fraction of the ‘blue’ MIR galaxies are currently on their first infall towards the cluster. The implications of adopting different SFR tracers for quantifying evolutionary trends like the Butcher-Oemler effect are also discussed.

Key words: galaxies: clusters: general, galaxies: evolution, galaxies: fundamental parameters, infrared: galaxies

1 INTRODUCTION

The Coma supercluster is the nearest rich supercluster of galaxies (Chincarini & Rood 1976; Gregory & Thompson 1978), con-

sisting of two rich Abell clusters, separated by $30 h_{70}^{-1}$ Mpc, but connected by a prominent filament of galaxies and poorer groups (e.g. Fontanelli 1984), which is part of the supercluster identified as the “Great Wall” in the first major redshift survey of galaxies in the nearby Universe (Geller & Huchra 1989). At a distance of $\sim 100 h_{70}^{-1}$ Mpc, it affords a closer look at the properties of indi-

^{*} e-mail: sm@star.sr.bham.ac.uk

vidual galaxies (1 kpc \simeq 2.1 arcsec), but its large angular scale on the sky presents observational challenges for the narrow fields of view of most instruments.

It is interesting to note that even though they are the two most significant structures in the supercluster, the two Abell clusters are remarkably different in every respect. The optical luminosity function of galaxies in the Coma cluster, for instance, has a much steeper faint-end slope than that of its neighbour Abell 1367 (Iglesias-Páramo et al. 2003). Early studies (e.g. Dressler 1980) revealed that the fraction of spiral galaxies in the Coma cluster is anomalously low compared to Abell 1367. In addition, galaxies in the core of the Coma cluster were identified to be unusually deficient in neutral hydrogen (e.g. Sullivan & Johnson 1978; Giovanelli & Haynes 1985; Bernstein et al. 1994), ionized hydrogen (Raychaudhury et al. 1997) and molecular gas (H_2/CO) (Boselli et al. 1997a). Bothun, Schommer, & Sullivan (1984) found a strong HI gradient in Coma galaxies- many of the inner, HI poor spirals being quite blue, suggesting that some gas removal process has acted quite recently, while Abell 1367 was found to be a mixture of HI poor and rich galaxies.

The availability of more detailed analyses of star formation, based on multi-wavelength data, and of spectral indices sensitive to stellar ages, has made this field more interesting. Estimates of star formation activity from mid-infrared (IR) (Boselli et al. 1997b) and Galaxy Evolution Explorer (*GALEX*) ultraviolet (Cortese, Gavazzi, & Boselli 2008) photometry show that star formation in Coma on the whole is substantially suppressed compared to that in the field, while Abell 1367 has an abundance of bright star-forming galaxies (Cortese, Gavazzi, & Boselli 2008).

In a hierarchical model of the formation of structures in the Universe, it is not surprising that a rich cluster, with a relaxed appearance in its X-ray image, such as Coma, would represent the end product of the gradual assimilation of several galaxy groups over time. In spite of the claim of Dressler & Shectman (1988) that the Coma cluster does not have significant substructure, it has subsequently been shown to have at least three major subclusters in the optical (e.g. West 1998) and X-ray maps (e.g. Davis & Mushotzky 1993; Adami et al. 2005). At the other end of the supercluster, Abell 1367 is also found to be elongated with three major subclusters, along the axis of the filament, with a population of star-forming galaxies infalling into the SE cloud and possibly the other two as well (Cortese et al. 2004). This has prompted a multitude of studies attempting to link the dynamical history of the supercluster with the properties of individual galaxies to investigate both the process of building clusters, as well as the effect of large-scale structure on the star formation history of galaxies (e.g. Haines et al. 2006).

By employing the spectral analysis of galaxies in Coma, together with the X-ray map of Neumann et al. (2003), Poggianti et al. (2004) found that the post-starburst (k+A) galaxies, in which star formation has been quenched within the last 1-1.5 Gyr, are associated with the X-ray excess attributed to the substructure in Coma. However, this work was limited to 3 fields in the ~ 2 Mpc region surrounding the centre of Coma.

In addition to star formation indices measured from optical spectra, the availability of *Spitzer* MIPS mid-IR observations has been recently utilised by several authors to characterise the star formation properties of the obscured component in galaxies in clusters and groups (e.g. Saintonge, Tran, & Holden 2008; Haines et al. 2009; Wolf et al. 2009; Bai et al. 2010), since the $24\mu\text{m}$ flux can be used as a representation of the dust-reprocessed overall IR flux.

Hereafter, we will refer to the pair of clusters Coma and

Abell 1367, along with the associated filament of galaxies as the Coma Supercluster. In this paper, we use the *Spitzer* MIPS $24\mu\text{m}$ observations, wherever available, along with the broadband colours and spectral star formation indicators from the Sloan digital sky survey (SDSS). We adopt the distance modulus of the Coma Supercluster to be $m - M = 35.0$, and use cosmological parameters $\Omega_\Lambda = 0.70$, $\Omega_M = 0.30$, and $H_0 = 70 \text{ km s}^{-1} \text{ Mpc}^{-1}$ for calculating the magnitudes and distances. We note that at the redshift of Coma ($z = 0.023$), our results are independent of the choice of cosmology. In the next section, we present our data and reduction methodology, and summarise our main results in §3 and §4. We discuss their implications, and compare the properties of galaxies in various parts of the supercluster in §5, summarising in §6.

2 OBSERVATIONAL DATA

We base our work on the photometric and spectroscopic data acquired by the SDSS Data Release 7 (Adelman-McCarthy et al. 2006, (DR7)), which for the first time covers the entire region of the Coma Supercluster presented in this paper. Over a smaller area, we also use archival $24\mu\text{m}$ mid IR (MIR) images, from the Multi-band Imaging Photometer (MIPS) instrument aboard *Spitzer* (Rieke et al. 2004), available over a significant fraction of the two main clusters.

2.1 Optical data

We select the galaxies belonging to the Coma supercluster from the SDSS spectroscopic catalogue only, requiring the member galaxies to be within $170.0 \leq \text{RA} \leq 200.0$ deg and $17.0 \leq \text{Dec} \leq 33.0$ deg on the sky, and with a radial velocity within $2,000 \text{ km s}^{-1}$ of the mean redshift of the Coma cluster ($6,973 \text{ km s}^{-1}$) or the Abell 1367 cluster ($6,495 \text{ km s}^{-1}$) respectively (Rines et al. 2003). All our galaxies are brighter than SDSS magnitude $r = 17.77$ ($\sim M^* + 4.7$ for Coma), which is the completeness limit of the SDSS spectroscopic galaxy catalogue.

2.2 MIPS $24\mu\text{m}$ data

For the mid-infrared study of Coma and Abell 1367, we use archival $24\mu\text{m}$ *Spitzer* MIPS data covering $2 \times 2 \text{ deg}^2$ in the case of Coma (PID: 83, PI G. Rieke) and $30' \times 30'$ for Abell 1367 (PID: 25, PI G. Fazio). The Coma $24\mu\text{m}$ dataset consists of four contiguous mosaics (see Fig. 1) obtained in medium scan mode, with scan leg spacing equal to the half array width, producing homogeneous coverage over the mosaic, with an effective exposure time per pixel of 88 sec. Bai et al. (2006), who used this data to determine the $24\mu\text{m}$ luminosity function of Coma, estimate the 80% completeness limit to be 0.33 mJy, corresponding to a star formation rate (SFR) of $0.02 M_\odot \text{ yr}^{-1}$ at the redshift of Coma. The Abell 1367 $24\mu\text{m}$ dataset consists of a single mosaic obtained in medium scan mode, with scan leg spacing equal to the full array width, producing an effective exposure time per pixel of 40 sec.

The SExtractor package (Bertin & Arnouts 1996) was used to automatically detect sources, and obtain photometric parameters. The images were first background-subtracted, and then filtered with Gaussian functions, with full width half maximum (FWHM) matching the $24\mu\text{m}$ point-spread function (PSF). Aperture photometry was obtained for all objects having 8 contiguous pixels above the 1σ rms background noise level. Following

SWIRE, we measured the fluxes within circular apertures of diameter 21, 30, 60, 90 and 120". For the vast majority of sources, the 6" FWHM point-spread function of MIPS leaves the object unresolved at 24 μ m, and hence we estimate the total 24 μ m flux of these objects from the flux contained within the 21" aperture, corrected by a factor 1.29.

However, at the redshift of the Coma and Abell 1367 clusters, many of the brighter galaxies (spirals in particular) are larger than our nominal 21" diameter aperture, such that a significant fraction of their 24 μ m flux is missed. For these galaxies, we use instead one of the larger apertures, matched to contain the optical flux as parametrized by R_{90z} (the radius which contains 90% of the z -band flux) as measured from the SDSS image. Finally, for some of the bright cluster galaxies (9 in total), the value of R_{90z} is under-estimated. To correct for this, SM eyeballed the 24 μ m images of these objects, and estimated an appropriate radius, in each case, for extracting the 'total' 24 μ m flux. In the case of the brighter spiral galaxies in Coma and Abell 1367, the 24 μ m emission often shows significant structure due to spiral arms and star-forming regions, necessitating a high value of the deblending parameter, to prevent the galaxy being shredded by SEXTRACTOR. Particular care was required to correctly deblend the face-on spiral NGC 3861 from NGC 3861B, while keeping NGC 3861 intact. We note that for $\sim 50\%$ of our sample the typical measurement error in the 24 μ m flux is < 0.1 mJy (which is $\lesssim 10\%$ of the measured flux), and for $> 95\%$ the error is < 0.35 mJy. In total, $\sim 90\%$ of our galaxies have 24 μ m flux measured with $< 30\%$ uncertainty.

2.3 Matching the SDSS spectroscopic catalogue with the 24 μ m sources

To match the SDSS spectroscopic catalogue for the Coma supercluster with the MIR 24 μ m data, we choose the nearest optical counterpart within 5" of each 24 μ m source. This accounts for a displacement of no more than $2.5 h_{70}^{-1}$ kpc between the centres. We note that $\gtrsim 80\%$ of the matches are found to have centres within 2" of each other. 16 of our sources above the detection threshold were found to have multiple matches within the matching radius of 5".

Our final dataset comprises of 3,787 galaxies ($r \leq 17.77$) with spectroscopic redshifts from SDSS, and radial velocity within $\pm 2,000$ km s $^{-1}$ of Coma or Abell 1367, in the ~ 500 square degree region of the sky covered by the Coma supercluster. Out of these, 197 within $\sim 2 h_{70}^{-1}$ Mpc of the centre of Coma and 24 within $\sim 0.65 h_{70}^{-1}$ Mpc of the centre of Abell 1367 are found to have a 24 μ m counterpart. The probability that a background MIPS source lies within the matching radius of 5" by chance, depends only on the density of the 24 μ m sources. For the completeness limit (0.33 mJy) adopted here, this density is $\sim 3,000$ deg $^{-2}$ (see fig. 3 of Shupe et al. 2008). This gives the required probability as 0.018, implying that our sample of 197 24 μ m detected galaxies in Coma may have 3–4 interlopers. A sample of the catalogue of data for the 24 μ m detected galaxies is provided in Table 1.

3 STAR FORMATION AND AGN ACROSS THE COMA SUPERCLUSTER

Located ~ 100 Mpc from us, the Coma supercluster offers a unique opportunity for investigating the effect on individual galaxies of the hierarchical formation of structures in the Universe, as galaxies progress through various environments towards the cores of the clusters.

In order to give a general overview of the optical star formation properties of galaxies along the entire supercluster, in Fig. 1 we plot the positions of all the galaxies from the SDSS spectroscopic catalogue found in our redshift range, and the major galaxy groups obtained from the NASA Extragalactic Database (NED, <http://nedwww.ipac.caltech.edu/>). In order to avoid multiple detections, we consider the groups only from the NGS, WBL, USGC and HCG catalogues, and even amongst these, we identify duplication by merging groups closer than 1' and within ± 100 km s $^{-1}$ of each other.

The positions of AGN host galaxies, identified using the BPT diagram (Baldwin, Phillips & Terlevich 1981, also see §4.2), and non-AGN starburst galaxies (star-forming on the BPT diagram, and having $\text{EW}(\text{H}\alpha) \geq 25 \text{\AA}$), are indicated in Fig. 1. We also show the limited regions at the cores of the Coma and Abell 1367 clusters, over which the 24 μ m data are available, and utilised in this paper. Plotted in the bottom panel of the same figure, is the distribution of the AGN and starburst galaxies, as fractions of the 150 galaxies contributing to each bin. It is worth mentioning that although these distributions are a fair representation of the data, the binning has resulted in a spurious feature at the position of Abell 1367. As is already well known in the literature, the central region of Abell 1367 is sparsely populated, the majority of galaxies in the core being late-type. In this figure, it appears that the fraction of starburst galaxies does not decline in the core of Abell 1367, but if the data is re-binned so as to have equally-spaced bins, this would not be the case. Having said that, the decline in the fraction of starburst galaxies at the centre of Abell 1367 is much shallower than that seen in Coma.

In general, the optically-identified AGN seem to be more or less uniformly distributed throughout the supercluster (Figs. 1 and 2), except for a sharp decline in the cores of both the clusters. This latter result is counter-intuitive, because AGN hosts are known to be early-type massive galaxies which mostly reside in dense environments. Hence, this may indicate that the optical emission from the AGN present in this region is obscured and/or detectable at other wavelengths (radio/X-ray). The latter is beyond the scope of this work, but our MIPS 24 μ m data supports the former possibility. As seen in Fig. 11, not only does the relative fraction of the red 24 μ m galaxies marginally increase towards the centre, around 50% of them are found within $0.5 h_{70}^{-1}$ Mpc of the centre of the Coma cluster, indicating that optical emission from several AGN hosts may be obscured. Further evidence in support of this argument may be drawn from Fig. 8 where a large fraction of galaxies detected at 24 μ m do not show [OIII] and/or H β in emission, but their H α /[NII] flux ratios are consistent with the presence of an AGN (Miller et al. 2003) on the BPT diagram (Baldwin, Phillips & Terlevich 1981).

We further investigate the environmental trends for AGN and star formation activity within the Coma supercluster, by estimating the local fraction of star-forming galaxies (f_{SF}) and AGN (f_{AGN}) over the entire supercluster, both for massive galaxies ($z < 14.5$; $M_z < M^* + 1.8$, assuming $M_z^* = -22.32$ from Blanton et al. 2001) and the dwarf galaxy population ($z > 15$; $M_z > M^* + 2.3$). Following Haines et al. (2007), we define the local projected density of galaxies ($\rho(\mathbf{x})$) using a variant of the adaptive kernel estimator (Silverman 1986; Pisani 1993), where each galaxy i is represented by an adaptive Gaussian kernel $\kappa_i(\mathbf{x})$. This is different from the algorithm of Silverman (1986), which, in its previous applications to astronomical data, requires the kernel width σ_i to be iteratively set to be proportional to $\rho_i^{-1/2}$. In this work, we fix the transverse width σ_i to be proportional to D_3 , where D_3 is the distance to the third nearest neighbour within 500 km s $^{-1}$.

Table 1. Catalogue of Coma galaxies detected at $24\mu\text{m}$ (This table is available in full online.)

RA (J2000)	Dec (J2000)	z	g mag	r mag	z mag	$24\mu\text{m}$ flux (mJy)	flag ^a
194.4574	28.6243	0.0250	17.80	17.35	17.24	0.31	1
195.1548	28.6641	0.0236	17.47	16.89	16.49	1.25	1
194.5385	28.7086	0.0255	15.21	14.56	14.08	36.02	1
194.9172	28.6308	0.0179	15.67	15.47	15.30	7.90	1
194.3645	28.4397	0.0260	17.16	16.57	16.19	0.75	1
194.5628	28.5218	0.0231	17.00	16.56	16.32	1.84	1
194.3912	28.4823	0.0209	14.35	13.54	13.00	1.86	3
194.4747	28.4998	0.0244	15.94	15.18	14.56	0.04	0
195.2170	28.3661	0.0255	14.51	13.73	13.10	1.39	0
195.3123	28.5217	0.0281	17.48	17.11	16.98	1.06	1

^a Classification on the basis of BPT diagram, where

0: unclassified

1: star-forming

2: AGN

3: AGN according to Miller et al. (2003) criteria (see text)

The dominant factors governing the star formation properties of a galaxy are the mass of its DM halo, and whether it is the central or a satellite galaxy in a halo (e.g. Kauffmann et al. 2004; Yang et al. 2005; Blanton et al. 2006). We adopt the above method, and choose the dimensions of the kernel, keeping this in mind. In the case of galaxies within groups or clusters, the local environment is measured on the scale of their host halo (0.1–1 Mpc), while for galaxies in field regions the local density is estimated by smoothing over their 5–10 nearest neighbours or on scales of 1–5 Mpc (for details, see Haines et al. 2007).

We can then map the local galaxy density (ρ) and z -band luminosity density (j_z) as $\rho(\mathbf{x}) = \sum_i \kappa_i(\mathbf{x}-\mathbf{x}_i)$ and $j_z(\mathbf{x}) = \sum_i L_{z,i} \kappa_i(\mathbf{x}-\mathbf{x}_i)$, where $L_{z,i}$ is the z -band luminosity of galaxy i (see Fig. 3). Following Yang et al. (2005), we identify local maxima in the z -band luminosity density as galaxy groups and clusters, whose masses correlate with the total z -band luminosity associated with the peak. By comparison with the Millennium simulation, we expect all groups with 4 or more members to be associated with a local maximum in $j_z(\mathbf{x})$ (Haines et al. 2007). The local z -band luminosity density is shown as black contours in Figs. 2–4.

In Fig. 2 we show the spatial variation of f_{AGN} among massive galaxies ($z < 14.5$) across the supercluster, where we calculate f_{AGN} as $\sum_{i \in AGN} \kappa(\mathbf{x}-\mathbf{x}_i) / \rho(\mathbf{x})$, where $i \in AGN$ is the subset of galaxies classified as optical AGN, based on the ratios of thermally excited and recombination lines used in the BPT diagram. We do not consider the lower mass galaxies, as the fraction of AGN declines rapidly to zero below $M_z > M^* + 2$;

For comparison, Fig. 3 shows the distribution of $f_{SF}(\mathbf{x})$ as $\sum_{i \in SF} \kappa(\mathbf{x}-\mathbf{x}_i) / \rho(\mathbf{x})$, where $i \in SF$ is the subset of galaxies classified as star-forming according to the line-ratios used in the BPT diagram. Fig. 4 shows a map of the local mean equivalent width (EW) of H α of star-forming galaxies as $\langle EW(H\alpha)(\mathbf{x}) \rangle = \sum_{i \in SF} EW(H\alpha) \kappa(\mathbf{x}-\mathbf{x}_i) / \sum_{i \in SF} \kappa(\mathbf{x}-\mathbf{x}_i)$, plotted in a manner analogous to that used by Haines et al. (2006) for galaxy colours in the Shapley supercluster.

In Fig. 2 we see that the AGN fraction f_{AGN} , among massive galaxies ($z < 14.5$) declines at the centre of the Coma and

Abell 1367 clusters, while elsewhere, it is uniformly distributed. This appears to contradict the results of Haines et al. (2007), who found the AGN fraction to be independent of environment, and to be a monotonically increasing function of stellar mass. However, the volume studied by Haines et al. (2007) within SDSS DR4 did not cover clusters as rich as Coma or Abell 1367. This may indicate that only the very dense environments affect the optical AGN activity of galaxies. The relation between f_{AGN} and local environment is unclear in the intermediate density group environment. While the f_{AGN} values decline in the centre of some groups, in others they exceed the mean value for the field. Although there is a slight indication that the groups in which the f_{AGN} appears to be declining, mostly lie on the filament connecting the Coma and Abell 1367, or in the vicinity of the clusters themselves, while the groups with higher values of f_{AGN} lie in underdense regions. However, it is not possible to draw any firm statistical inferences from this observation.

Whether the AGN fraction f_{AGN} varies with environment or not depends on how the activity of the galactic nuclei is defined. Miller et al. (2003) do not find any correlation between galaxy density and f_{AGN} in a large sample of galaxies ($M_r = -20$; $0.05 < z < 0.095$), where the AGN are defined in terms of optical emission line ratios characterised by the BPT diagram. Other studies find higher incidence of optical AGN in groups and clusters (Arnold et al. 2009). If the AGN were selected according to their radio, mid-IR or X-ray properties, they would be found in different hosts: radio AGN in early-type galaxies, IR AGN in bluer galaxies, and X-ray AGN in galaxies of intermediate colour (Hickox et al. 2009). The environment dependence of AGN activity is thus largely linked to the distribution of the hosts. The incidence of X-ray AGN is higher in galaxy groups than in galaxy clusters (Martini et al. 2006; Shen et al. 2007). The fraction of radio-loud AGN is the same in the brightest galaxies of groups and clusters and in the field, but higher in non-central galaxies (Best et al. 2005). Del Pozzo et al. (2010) show that the mass function of black holes is independent of environment, and the variation in the distribution of optical, radio and X-ray AGN can be understood in terms of the accretion processes

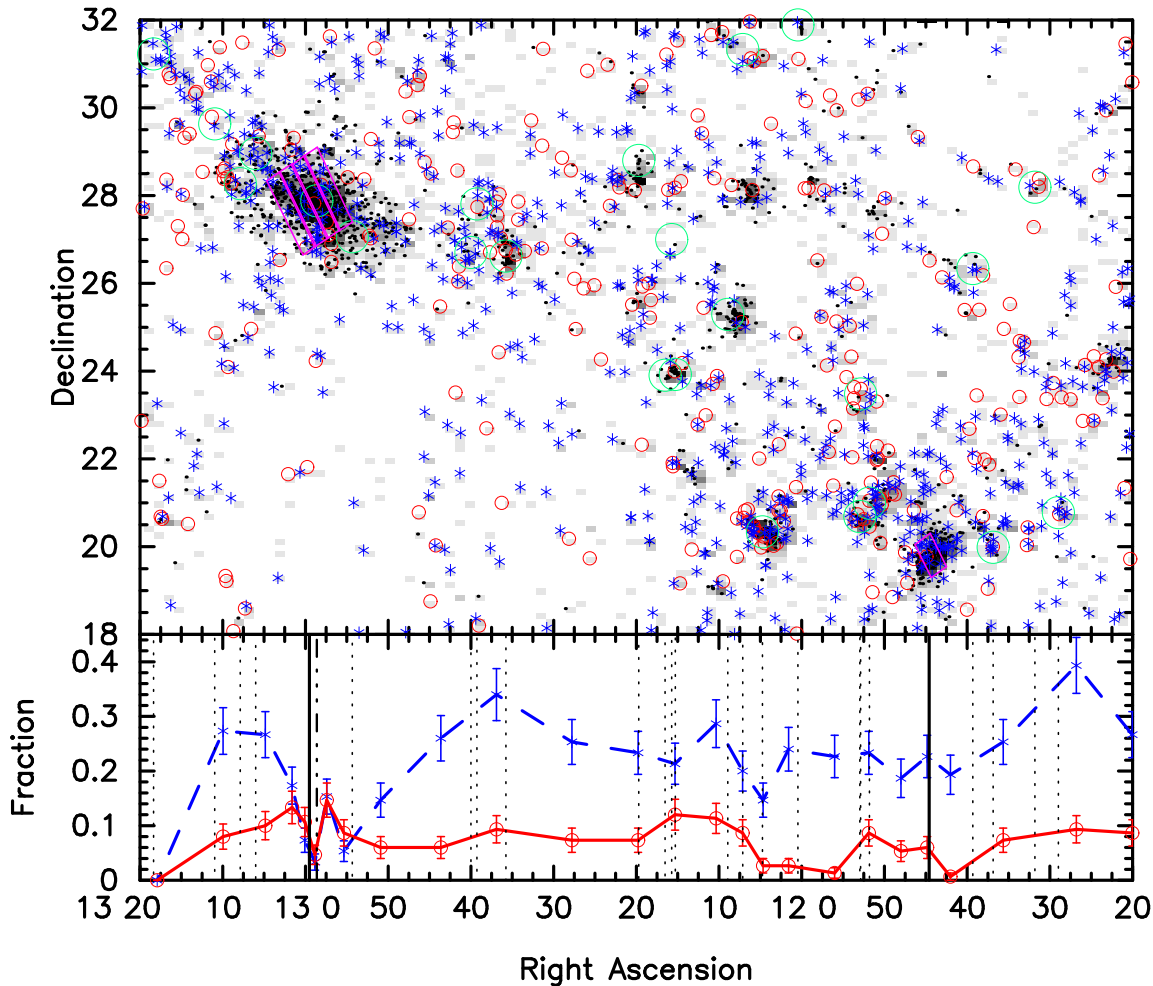


Figure 1. **Top panel:** The surface density of galaxies in the Coma supercluster is shown in *grey*. The positions of passive galaxies (*black dots*), AGN host galaxies (*open red circles*) and starburst galaxies (*blue stars*); $\text{EW}(\text{H}\alpha) \geq 25\text{\AA} \sim \log \text{SSFR} \sim -10\text{yr}^{-1}$ are indicated. The *big green circles* are the groups in the region, from the NASA Extragalactic Database. The rectangular pink regions show the Spitzer MIPS fields of view for the two clusters. **Bottom panel:** The *solid red line* and the *dashed blue line* show the fraction of AGN and of the starburst galaxies, among all the galaxies shown in the upper panel. The bins are chosen to have 150 galaxies in each of them. The *solid vertical lines* represent the centres of the Coma cluster and Abell 1367 respectively, while the *dot-dashed line* shows the RA position of the NGC 4839 group (see text). All the dotted lines represent the positions of groups, shown in the upper panel.

that lead to the manifestation of the AGN in the various ranges of electromagnetic radiation.

We measured the significance of the spatial variations seen in f_{AGN} across the supercluster by performing Monte Carlo simulations, in which we made repeated maps of f_{AGN} after randomly assigning the positions of the AGN to the bright galaxies (i.e. testing the null hypothesis that f_{AGN} is constant across the supercluster), and measuring the fraction of maps in which a given local value of f_{AGN} was obtained within one of the Monte Carlo simulations. The results of these simulations are represented by the white contours, which indicate regions that have $f_{\text{AGN}} = 1$ and $2\text{-}\sigma$ below the mean value across the supercluster. This confirms that the decline in f_{AGN} seen towards the core of the Coma cluster is significant at the 3σ level, while that seen in Abell 1367 is significant at the 2σ level.

In Fig. 3 we show the general correlation between the fraction of star-forming galaxies (f_{SF}) and environment for massive galaxies ($z < 14.5$; top panel) and the dwarf galaxies ($z > 15$; bottom panel). For the massive galaxies we find an almost uniform $f_{\text{SF}} < 0.5$ in all the environments. For dwarf galaxies, we see a

much stronger SF-density relation, with f_{SF} rising rapidly from the $f_{\text{SF}} < 0.1\text{--}0.4$ seen in the cluster cores, to $f_{\text{SF}} > 0.95$ in the field. This result is in agreement with literature, where, using colour or SFR indicators, it has been shown that dwarf galaxies exhibit much stronger radial trends with environment than their massive counterparts (Gray et al. 2004; Tanaka et al. 2004; Smith et al. 2006; Haines et al. 2007, among others). The origin of the SF-density relation for the dwarf galaxies can be attributed to the fact that (i) the star formation in dwarf galaxies can easily be quenched by the tidal impact of a massive neighbour and/or the ICM of the cluster (e.g. Larson, Tinsley & Caldwell 1980), and (ii) unlike their massive counterparts, dwarfs (of the luminosities considered here) do not become passive by internal mechanisms such as gas consumption through star formation, merging etc.. However, the effects of supernovae wind blowouts and feedback become significant for relatively faint ($M^* \lesssim 10^7 M_{\odot}$) dwarfs (e.g. Mac Low & Ferrara 1999; Marcolini et al. 2006). In this work we do not find any evidence for the quenching of star formation in galaxies on the filament(s), but only in the cores of the embedded galaxy groups.

The $\text{H}\alpha$ emission traces the current SFR of a galaxy, while

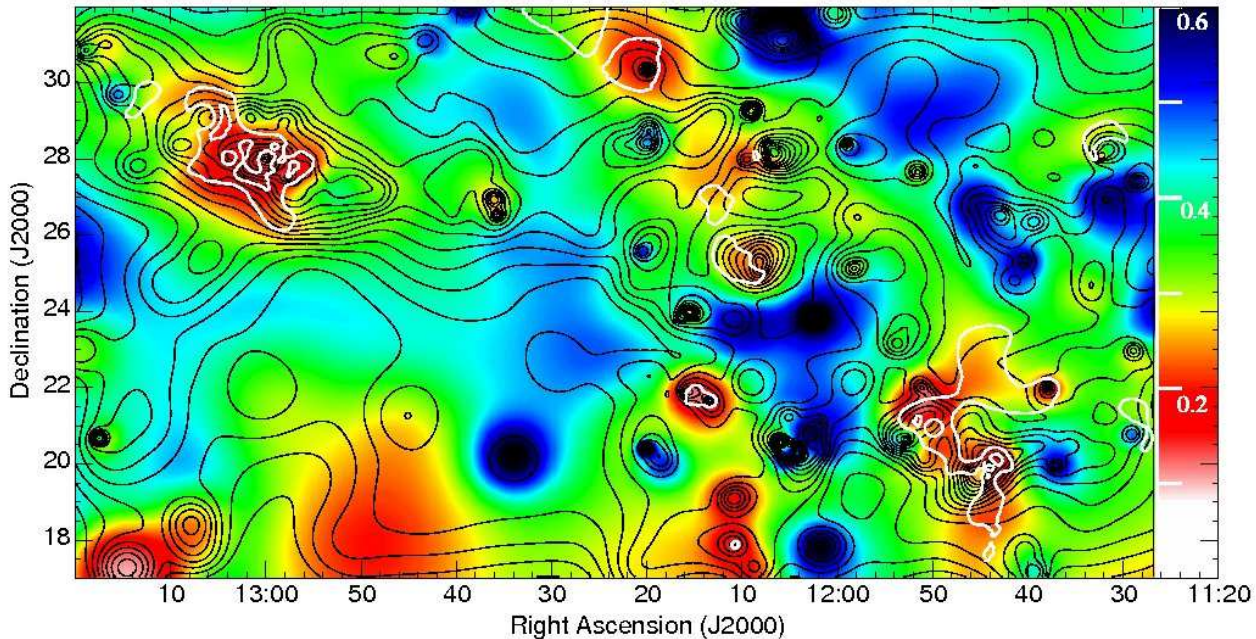
AGN fraction among massive ($z < 14.5$) galaxies

Figure 2. The local AGN fraction (f_{AGN}) among massive galaxies ($z < 14.5$), as a function of spatial position across the Coma supercluster. The map is colour-coded with f_{AGN} . The *black contours* indicate the local luminosity-weighted (z -band) galaxy density across the supercluster. The *white contours* indicate regions with AGN fraction $f_{AGN} = 1$ and $2\text{-}\sigma$ below the mean value over the supercluster.

the continuum flux under this line can be used as an indicator of its past SFR, making the globally averaged $\text{EW}(\text{H}\alpha)$ from a galaxy an effective indicator of the birthrate parameter ($b \equiv$ current SFR normalized by the SFR averaged over the lifetime of a galaxy). Recently, Lee et al. (2009) have shown that $\text{EW}(\text{H}\alpha) \sim 40\text{\AA}$ corresponds to $b = 1$. In Fig. 4 we show the variation in the mean $\text{EW}(\text{H}\alpha)$ as a function of environment for the star-forming dwarf galaxies. This is potentially a very powerful technique for dissociating the intrinsically active star formation history (SFH) of low-mass galaxies from a starburst caused by the impact of local environment (see Haines et al. 2007, for instance).

If galaxies are slowly quenched by interactions with their environment (Balogh et al. 2004a), a decline in the mean $\text{EW}(\text{H}\alpha)$ is expected in the regions of denser environment. On the other hand, if star formation is triggered due to the impact of environment, the mean $\text{EW}(\text{H}\alpha)$ should increase. Unlike the slow quenching of dwarfs in the dense environments (Tanaka et al. 2004; Haines et al. 2007), here, in the Coma supercluster, we find that the dwarf galaxies follow different evolutionary paths in the groups and in the denser cluster environments. In galaxy groups, a dwarf galaxy is slowly quenched via interactions with the other group members and/or the tidal field of the group, while in the clusters, an infalling dwarf experiences a starburst in the intermediate density environment at the cluster periphery (Porter et al. 2008; Mahajan, Raychaudhury & Pimblett 2010), and is then rapidly quenched via cluster-related environmental mechanisms, such as ram-pressure stripping.

In analogy to Fig. 2, we measure the significance of the spatial variations seen in the mean $\text{EW}(\text{H}\alpha)$ via Monte Carlo simulations, this time by making repeated maps after randomly swapping the values of $\text{EW}(\text{H}\alpha)$ among the dwarf star-forming galaxies. In doing

this, we seek to test the null hypothesis that the $\text{EW}(\text{H}\alpha)$ is independent of spatial position among star-forming galaxies. In Fig. 4, we show, as overlaid white contours, the regions in which the local observed mean value of the $\text{EW}(\text{H}\alpha)$ is 2 and 3σ above that averaged over the whole supercluster. This confirms that the excess star formation seen in the infall regions of Coma, and towards the core of Abell 1367, is indeed significant at $> 3\sigma$ level. In quantitative terms, this excess in the infall regions of the Coma cluster is due to a population of ~ 30 dwarf starburst galaxies ($z > 15$, $\text{EW}(\text{H}\alpha) > 40\text{\AA}$) located within or along the white $2\text{-}\sigma$ contours in Fig. 4. The analogous excess in the core of Abell 1367 can be ascribed to ~ 10 starburst dwarf galaxies.

4 OPTICAL AND MID-IR ANALYSIS OF COMA AND ABELL 1367 GALAXIES

The infrared (IR) emission from normal galaxies around $\lambda = 24\mu\text{m}$ is dominated by hot dust in the HII regions of massive stars, in addition to (usually) minor contribution from asymptotic giant branch (AGB) stars and the general interstellar medium (ISM). This recycled emission, together with the optical emission, can thus provide a good estimate of the total starlight of a galaxy and be used to better constrain the current and past star formation rate (SFR) of a galaxy (Calzetti et al. 2007; Kennicutt et al. 2009; Rieke et al. 2009, among others). While IR astronomers usually study late-type galaxies, early-type galaxies have received sporadic attention only in the context of the warm dust component detected in a few of them (e.g. Knapp et al. 1989).

In this paper, we combine the optical photometric and spectroscopic data taken by the SDSS DR7, with the $24\mu\text{m}$ *Spitzer*/MIPS data, which is sensitive to processed optical emission from stars, to

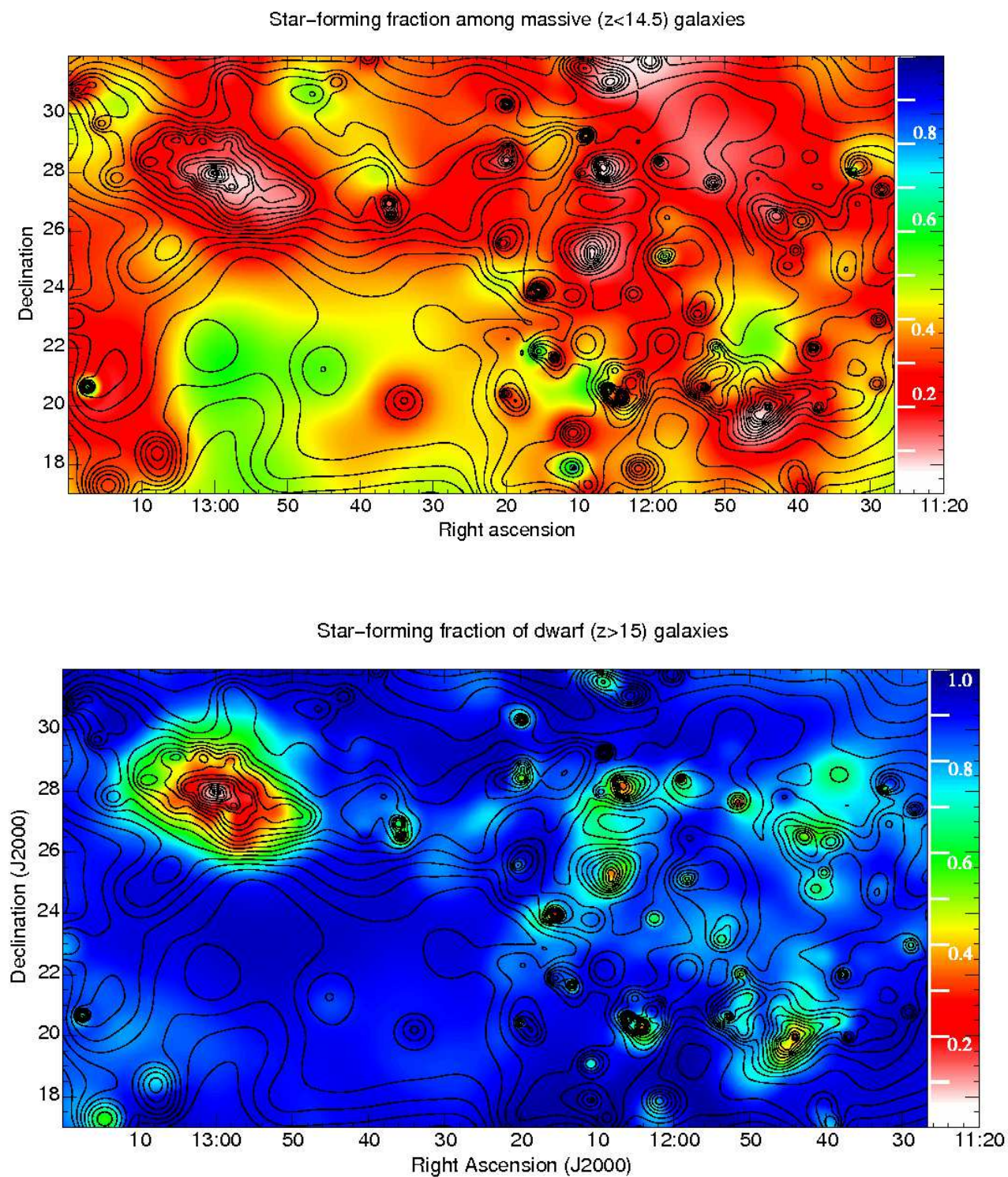


Figure 3. The local fraction of star-forming galaxies (f_{SF}) as a function of spatial position across the Coma supercluster, for massive galaxies ($z < 14.5$; top panel) and dwarf galaxies ($z > 15$; lower panel). The colours indicate f_{SF} , and the same colour scale is used in both the panels. Overlaid are black contours indicating the z -band luminosity-weighted galaxy density across the supercluster. This figure shows that in the Coma supercluster, star formation in the massive galaxies ($z < 14.5$) seems to be suppressed independent of their local environment, while the dwarf galaxies ($z > 15$) are star-forming everywhere except in the dense environment in the vicinity of rich clusters and galaxy groups.

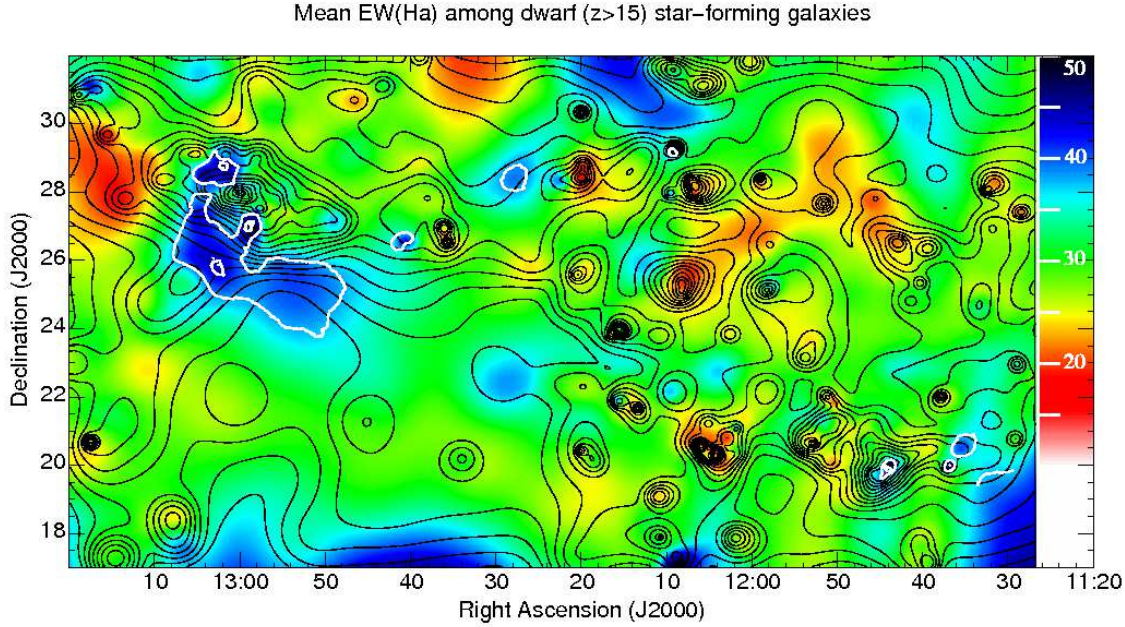


Figure 4. The local mean H_{α} equivalent width of star-forming ($EW(H_{\alpha}) > 2\text{\AA}$) dwarf ($z > 15$) galaxies across the Coma supercluster, indicated by colour. Overlaid are *black contours* indicating the z -band luminosity-weighted galaxy density across the supercluster, and *white contours* showing regions where the local observed mean value of the $EW(H_{\alpha})$ is 2 and 3- σ above that averaged over the whole supercluster.

study the star formation activity of galaxies residing in the denser regions of the Coma supercluster.

4.1 Optical and MIR colours

In Fig. 5, we show the colour magnitude relation (CMR) for all the spectroscopic galaxy members ($r \leq 17.77$) found in this region in the SDSS DR7, and those that are also detected at $24\mu\text{m}$ in the *Spitzer*/MIPS observations. For comparison, the $24\mu\text{m}$ galaxies found in Abell 1367 are also shown. We only use galaxies brighter than $r = 15.5$ to fit the CMR. The CMR is of the form $g-r = 1.244 - 0.032 r$ for all the Coma galaxies, where the mean absolute deviation from the relation is ± 0.064 mag.

We repeat this analysis in Fig. 6 for the near-infrared (NIR) band of SDSS (z -band), and the $24\mu\text{m}$ MIPS band. The galaxies classified as red and blue on the optical colour-magnitude diagram, split into two separate classes around $(24-z) = -6$ mag on the plot of the near/mid IR colour and magnitude as well. Although we overplot the lines of constant SFR in Fig. 6, according to the empirical relation given by Calzetti et al. (2007), it is important for the reader to consider that the $24\mu\text{m}$ flux alone is an accurate SFR indicator only for the late-type, dusty star-forming galaxies (we return to this issue below). The SDSS z -band, centred at $\sim 9000\text{\AA}$, is a good measure of the light from evolved stars, and hence the stellar mass of a galaxy. The top axis shows the stellar mass of galaxies estimated using the relation $\log M^* = -0.306 + 1.097(g-r) - 0.1 - 0.4(M_r - 5 \log h - 4.64)$, from Bell et al. (2003). On the other hand, the $24\mu\text{m}$ MIPS band in the MIR is a good proxy for the dust-processed light. This makes the $(24-z)$ colour an excellent approximation for the value of the specific star formation rate (SSFR or SFR/M^*) of galaxies.

Figs. 5 and 6 together show that the $24\mu\text{m}$ detected red se-

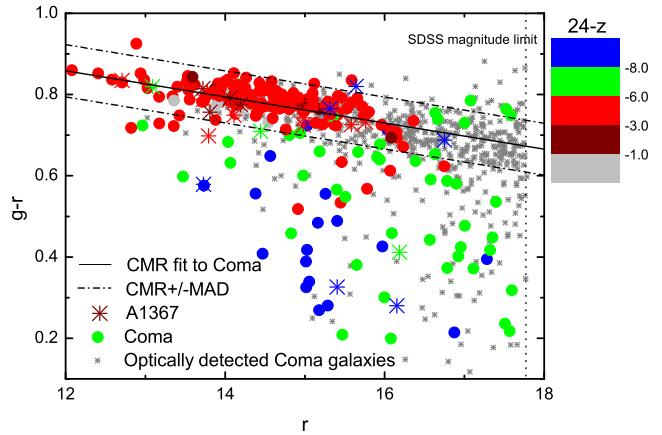


Figure 5. The $(g-r)$ vs r colour-magnitude relation for the $24\mu\text{m}$ bright galaxies detected in the Coma cluster (*circles*) and Abell 1367 (*big stars*). The solid line shows the colour-magnitude relation (CMR) fitted to the Coma data points, while the dot-dashed lines mark the mean absolute deviation (MAD) boundaries on either side. We adopt the lower MAD boundary in $(g-r)$ for segregating the red sequence from the blue cloud. Note that we do not use any upper bound for the red sequence because fitting is done using spectroscopically confirmed cluster members only. The symbols are colour-coded according to the $(24-z)$ colour of the MIR bright sources (Fig. 6). All the other Coma galaxies are shown as *grey stars*. Note that $(24-z) = -6$ mag separates the red sequence galaxies from the blue ones in a $z-(24-z)$ plane (Fig. 6).

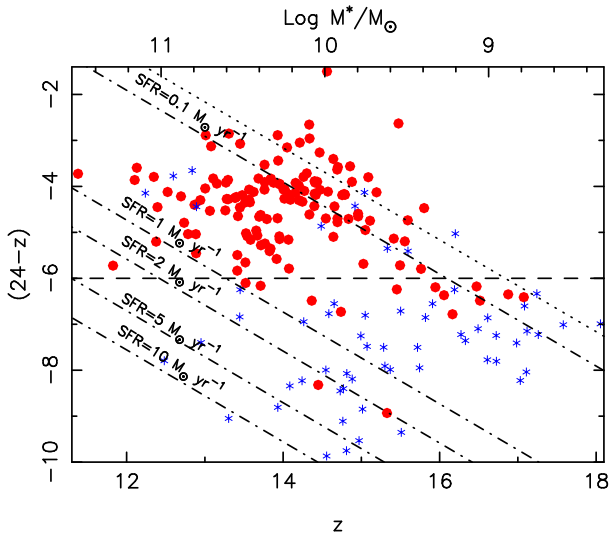


Figure 6. The $(24-z)$ colour of all galaxies in the Coma supercluster sample, divided into blue cloud (blue stars) and red sequence (red) (Fig. 5) galaxies, are plotted against their z -band magnitudes. The dotted line shows the 80% completeness limit of the $24\mu\text{m}$ data. The constant SFR lines are drawn using the conversion factor given by Calzetti et al. (2007). The horizontal dashed line at $(24-z) = -6$ mag is our empirically chosen criterion for selecting star-forming galaxies. The top axis shows the stellar mass of galaxies estimated using a relation from Bell et al. (2003).

quence galaxies in Coma have consistent optical and MIR colours. We note that the optical-MIR colours of the red sequence galaxies are not consistent with those expected from photospheric emission from old stellar populations, with an excess emission always apparent at $24\mu\text{m}$. The *Spitzer* Infrared Spectrograph observations of early-type galaxies in Virgo and Coma clusters show that the diffuse, excess emission, apparent at $10\text{--}30\mu\text{m}$ in these galaxies, is due to silicate emission from the dusty circumstellar envelopes of mass-losing evolved AGB stars (Bressan et al. 2006; Clemens et al. 2009). The strength of this silicate emission is a slowly declining function of stellar age (Piovan, Tantalo & Chiosi 2003), and persists even for very evolved stellar populations (> 10 Gyr). The optical-MIR colours of Virgo and Coma galaxies have been found to be consistent with such old stellar populations (Clemens et al. 2009).

The blue galaxies in Fig. 5 have a wide spread in both colour and magnitude. The inhomogeneity of this class of galaxies becomes even more clear in Fig. 7, where we plot the optical ($g-r$) colour against the near/mid-IR $(24-z)$ colour. Just as in Fig. 5, the passive red galaxies cluster in a small region of the colour-colour space, but the blue galaxies and (optical) AGNs span a wide range along both the axes. We note the clear separation of star-forming (blue stars) and passive (red points) galaxies in $(24-z)$ colour. The horizontal dashed line in Fig. 7 indicates our empirically chosen criterion to separate the two populations about $(24-z) = -6$. Interestingly, although the AGN and star-forming galaxies (green and blue symbols respectively) are classified on the basis of their optical spectra on the BPT diagram (Baldwin, Phillips & Terlevich 1981, also see §4.2), they occupy distinct regions in this plot of optical vs optical-IR colour, as well.

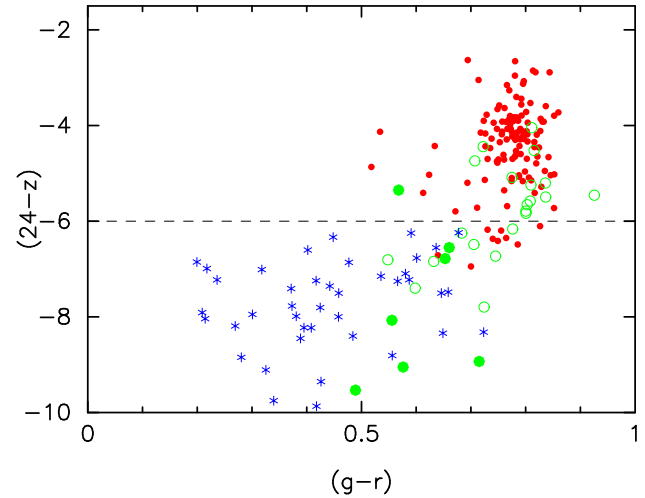


Figure 7. This colour-colour diagram shows that the galaxies identified as AGN (green circles) and star-forming (blue stars), on the basis of the BPT diagram according to their optical spectra (see Fig. 8), occupy different regions on the near/mid IR magnitude-colour diagram. The solid and open green circles represent AGN classified on the BPT diagram and by the Miller et al. (2003) criterion respectively (see text). The passive galaxies (red points) detected at $24\mu\text{m}$ are concentrated in a small region on the top right of the diagram. The horizontal line at $(24-z) = -6$ mag marks the boundary between these two classes in the z - $(24-z)$ IR colour magnitude space (Fig. 6).

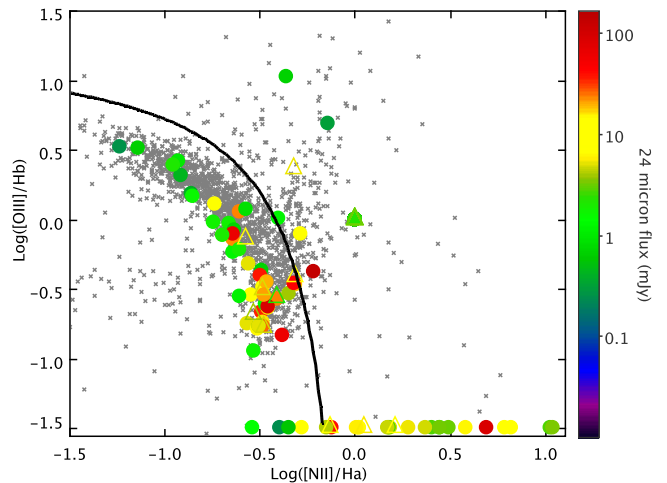


Figure 8. The BPT diagram (Baldwin, Phillips & Terlevich 1981) for the $24\mu\text{m}$ detected galaxies in the Coma cluster (filled circles) and in Abell 1367 (open triangles), colour coded by their $24\mu\text{m}$ flux. We also plot all the galaxies within $\pm 2,000$ km s^{-1} of Coma or Abell 1367, in the 500 square degree supercluster region, but not detected at $24\mu\text{m}$, as grey crosses. The points plotted in a line at $\log[\text{OIII}]5007/\text{H}\beta = -1.5$ are the galaxies which have no detected [OIII] and/or $\text{H}\beta$ emission. It is interesting to observe that a large fraction of the Coma galaxies without [OIII] and/or $\text{H}\beta$ have their [NII]/ $\text{H}\alpha$ flux ratios as expected for AGN, suggesting that these galaxies may have their nuclear emission obscured. We classify such galaxies as AGN if they have $\text{Log}([\text{NII}]/\text{H}\alpha) > -0.2$ (Miller et al. 2003).

4.2 Optical and $24\mu\text{m}$ star formation indicators

The understanding of the formation of stars in galaxies requires, among other things, the measurement of the rate at which the interstellar gas is converted into stars. With the development of appropriate technology, radio, IR and UV photometry and spectroscopy are increasingly being employed, in addition to the traditional optical observations, for the purpose of measuring the rate of star formation. The dust clouds surrounding the young stellar concentrations absorb starlight and re-radiate it at IR wavelengths. Thus, the SFR measured by IR measurements is accurate only in the optically thick limit. The observed UV radiation escaped from the molecular clouds which block the UV light at earlier ages, comes mostly from stars with ages $10^7 - 10^8$ yrs (Calzetti et al. 2005). $\text{H}\alpha$ emission is produced only in the first few million years from the most massive stars (Leitherer et al. 1999). Indeed, a combination of UV, $\text{H}\alpha$ and IR observations is required to give a full measure of the obscured and unobscured star formation. In this section, we attempt to combine the direct (optical) and the obscured (IR) radiation from the Coma and Abell 1367 galaxies to understand the process of star formation across this supercluster.

The $24\mu\text{m}$ IR emission in galaxies can result from dust heated by young massive star clusters as well as the AGN. Since our MIPS data comes from the densest regions at the core of the Coma cluster (Fig. 1), which is a favourable environment for AGN hosts, it is important to investigate the origin of the $24\mu\text{m}$ emission in these galaxies. To do so, in Fig. 8 we plot the usual ratios of optical emission linewidths ([OIII], $\text{H}\beta$, [NII] and $\text{H}\alpha$), known to distinguish star forming galaxies from those dominated by AGN, in what is popularly known as the BPT diagram (Baldwin, Phillips & Terlevich 1981).

In Fig. 8, we show all the emission-line galaxies found in the $\pm 2,000 \text{ km s}^{-1}$ redshift slice around Coma and/or Abell 1367, in the ~ 500 square degrees Coma supercluster region (see Fig. 1), along with the galaxies detected at $24\mu\text{m}$ (MIPS) in Coma (circles) and Abell 1367 (open triangles). Although we find a significant number of $24\mu\text{m}$ detected galaxies with [NII]/ $\text{H}\alpha$ ratios suggestive of AGN, this does not mean that the $24\mu\text{m}$ emission is predominantly due to AGN. Goulding & Alexander (2009) have tried to estimate the contribution of the AGN component to the IR emission from galaxies using Spitzer/IRS spectroscopy. Although only a few galaxies in their sample have IR fluxes produced predominantly by AGN, they also find that a substantial fraction of AGN are optically obscured, consistent with the results presented here.

We find that most of the galaxies which have measured values of all four emission lines are dusty star forming galaxies. However, interestingly, a large number of galaxies detected at $24\mu\text{m}$ in Coma that do not show emission in [OIII] and/or $\text{H}\beta$, do have a [NII]/ $\text{H}\alpha$ flux ratio consistent with the presence of an AGN. Such galaxies can be classified as AGN if $\log([\text{NII}]/\text{H}\alpha) > -0.2$ (Miller et al. 2003).

The EW of the Balmer lines, especially that of the $\text{H}\alpha$ emission line, has been extensively used to estimate the current optical SFR of galaxies. It has been shown in the literature that the $24\mu\text{m}$ flux is a good measure of dust-processed star light (e.g. Calzetti et al. 2007). But, the $24\mu\text{m}$ observations used in this work cover the very central regions of the Coma cluster, and Abell 1367, which comprises mostly of early-type galaxies. In order to test the correspondence between the direct and dust-processed SFR tracers, in Fig. 9 we plot the $(24-z)$ colour as a function of spectroscopically measured $\text{EW}(\text{H}\alpha)$. We also colour-code the symbols according to the concentration parameter of the galaxies (ratio of the

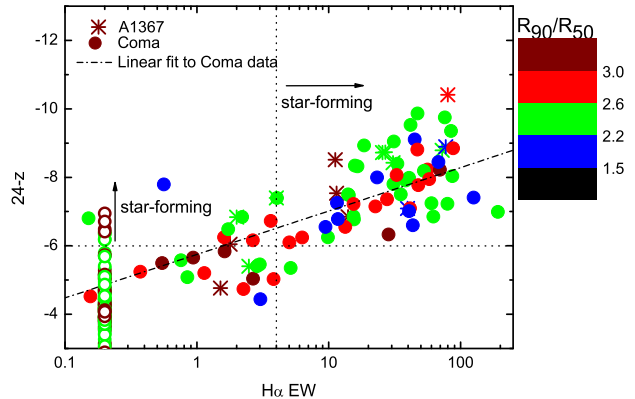


Figure 9. The $(24-z)$ colour as a function of $\text{H}\alpha$ EW for Coma (filled circles) and Abell 1367 (stars) galaxies respectively. The straight line represents the linear fit to galaxies in the Coma cluster. Though there is a considerable scatter, the correlation between the two quantities is significant. The dotted lines represent the lower limits adopted to select star-forming galaxies using ($\text{H}\alpha$ EW = 4\AA) and $(24-z)$ colour = -6.0 (see Fig. 6). For completeness, we also show the $24\mu\text{m}$ detected galaxies that do not have $\text{H}\alpha$ emission in SDSS spectra at $\text{EW}(\text{H}\alpha) = 0.2\text{\AA}$ (open circles). The $24\mu\text{m}$ emission in these galaxies is likely to come from the evolved AGB stars.

Petrosian radii R_{90r}/R_{50r} from the SDSS photometric catalogue, which is an indicator of morphology). Passive spirals often have concentration indices consistent with early-types ($R_{90r}/R_{50r} > 2.6$; also see Mahajan & Raychaudhury 2009). But Fig. 9 shows that both the spiral and spheroidal galaxies are uniformly distributed along both the axes, implying that the emission-line galaxies detected at $24\mu\text{m}$ at the core of Coma and Abell 1367 are not dominated by galaxies of any particular morphological type (as quantified by the concentration index).

Due to the dominance of early-type galaxies in our $24\mu\text{m}$ sample, it is not surprising that only a small fraction of galaxies classified as star-forming on the basis of their $(24-z)$ colour (Fig. 6), show no signs of current star formation in their optical spectra. For completeness, at $\text{EW}(\text{H}\alpha) = 0.2\text{\AA}$ we plot all the $24\mu\text{m}$ detected galaxies that do not show optical emission in $\text{H}\alpha$. As expected, most of these galaxies have $(24-z)$ colours and concentration parameters consistent with those of quiescent early-type galaxies. This suggests that their $24\mu\text{m}$ emission is primarily due to the contribution from AGB stars, which (unlike young stars) do not produce $\text{H}\alpha$ emission. The good overall correspondence between the photometric $(24-z)$ colour and spectroscopic $\text{EW}(\text{H}\alpha)$ makes the $(24-z)$ colour a good candidate for comparing the star formation activity in nearby galaxies, in the absence of optical spectra.

4.3 Varying fractions of star-forming galaxies with SFR tracer: implications for the Butcher-Oemler effect

Photometric colours and EWs of emission lines like [OII] and $\text{H}\alpha$ have been extensively used for studying the evolution of galaxies in time and across the sky. In one such pioneering work, Butcher & Oemler (1984, BO84) found that clusters at moderate to high redshifts contain an ‘excess’ of blue galaxies, relative to their local counterparts. They estimated the blue fraction by considering galaxies found within R_{30} (radius containing 30% of all

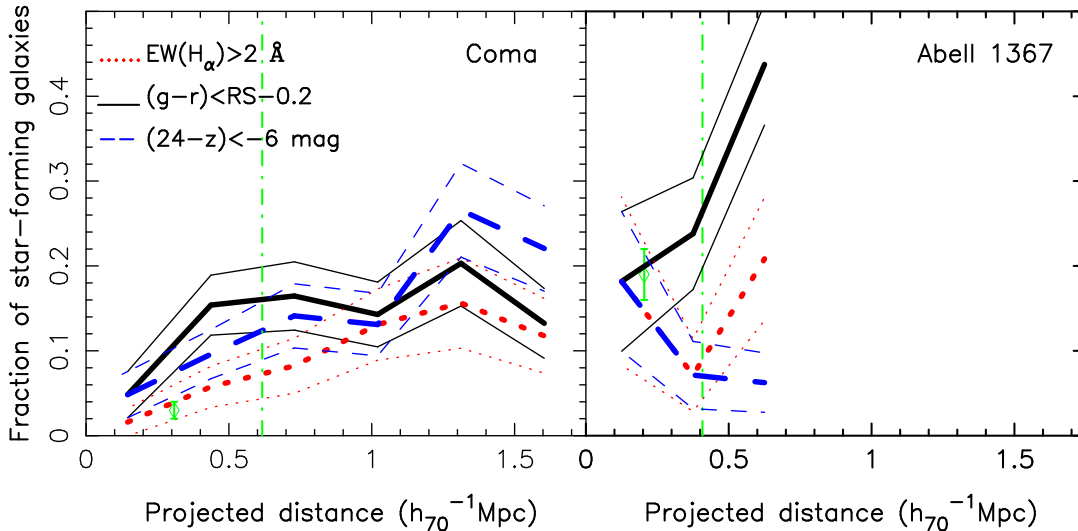


Figure 10. The fraction of star-forming galaxies as a function of (projected) cluster-centric radius for Coma in the **Left** panel and Abell 1367 on the **Right**. In both panels, the *solid black line* shows the radial variation in the fraction of star-forming galaxies, selected using the $(g-r)$ colour threshold, the *dotted red line* makes use of the H_α EW ($\geq 2\text{\AA}$) and the *dashed blue line* represents the same, for star-forming galaxies chosen by the $(24-z) < -6$ criterion. The corresponding *thin curves* show the $\pm 1\sigma$ Poisson scatter. In all cases, all the spectroscopically identified galaxy members with $M_z < -20.82$ ($M_z^* + 1.5$; see text), and l.o.s. velocity $\pm 3,000$ km s $^{-1}$ of Coma and/or Abell 1367, are used to estimate the fractions. For Abell 1367, we show galaxies only within the region, of scale $\sim 0.75 h_{70}^{-1}$ Mpc, for which the $24\mu\text{m}$ data is available. This diagram shows the importance of taking account of the star formation activity used to quantify and understand evolutionary trends, such as the Butcher-Oemler effect. For comparison, the R_{30} radius adopted by Butcher & Oemler (1984), and the fraction of blue galaxies found in Coma and Abell 1367, are also shown by the vertical *dot-dashed lines* and *open green diamonds* respectively.

red sequence galaxies), for which the optical broadband colours are bluer by at least 0.2 mag than that of the red sequence galaxies. For the redshift regime of Coma (≤ 0.1), BO84 found a uniform blue fraction within R_{30} . Since then, several such studies have sought to quantify and validate the Butcher-Oemler effect for different samples of clusters. Some of these define their samples in a way similar to that of BO84, and obtain similar results (e.g. Margoniner & Carvalho 2000).

Using panoramic MIR data for 30 clusters (including both Coma and Abell 1367) over $0 < z < 0.4$, Haines et al. (2009) are able to reproduce the Butcher-Oemler effect using a fixed limit in L_{IR} ($5 \times 10^{10} L_\odot$) (equivalent to a fixed SFR of $8 M_\odot \text{yr}^{-1}$), but show that the Butcher-Oemler effect can be largely explained as a consequence of the *cosmic* decline in star formation (Le Floch et al. 2005; Zheng et al. 2007). In this case, the blue galaxies in clusters are those that are recently accreted from the field (accretion has occurred at a relatively constant rate since $z \sim 0.5$; Berrier et al. 2009), but since the global level in star formation among these galaxies has declined, a smaller fraction of the infalling population is classed as blue (which assumes a non-evolving level of star formation), resulting in the observed Butcher-Oemler effect.

Elsewhere (Balogh, Navarro, & Morris 2000; Ellingson et al. 2001; De Propris et al. 2004), studies going out to several multiples of the cluster-centric radius, scaled by R_{200} , show the effect of the chosen aperture size on the blue fraction. It has been shown that the observed gradual radial trend of f_{SF} is consistent with a simple infall scenario, whereby the star-forming galaxies are infalling field galaxies, which are then quenched rapidly upon their first passage through the cluster core (e.g. Balogh, Navarro & Morris 2000; Ellingson et al. 2001; Haines et al. 2009). By comparing the photometric colour with the spectroscopically determined SSFR, Mahajan & Raychaudhury (2009) show that the presence of metal-rich stellar populations in low redshift cluster galaxies can also in-

fluence the evolutionary trends such as the Butcher-Oemler effect, if they are studied only using galaxy colours. Several recent studies indicate that a non-negligible fraction of red sequence galaxies show signs of ongoing star formation from their optical spectra and/or broad-band colour, and that a robust separation of passive and star-forming galaxies requires mutually independent data (e.g. Bildfell et al. 2008). In this work, we show that in the Coma Supercluster, the value of f_{SF} not only varies with the cluster-centric aperture used for measuring the blue fraction, but can also be severely effected by the SFR tracer employed.

In Fig. 10 we plot the fraction of non-AGN, star-forming galaxies found using 3 different criteria: (i) IR colour [$(24-z) \leq -6$ mag; Fig. 6], (ii) $EW(H_\alpha) \geq 2\text{\AA}$ and, (iii) the photometric colour $(g-r)$ is bluer than that of the fitted red sequence (Fig. 5, by more than the mean absolute deviation, for all the Coma and Abell 1367 galaxies. BO84 had included galaxies brighter than $M_V = -20$ ($H_0 = 50$ km s $^{-1}$ Mpc $^{-1}$) in their sample. To make a fair comparison with the work of Butcher & Oemler (1984), without adding uncertainties by using empirical relations to convert magnitudes from one passband to the other, in Fig. 10 we choose to only include galaxies brighter than $M_z^* + 1.5$ ($M_z^* = -22.32$; Blanton et al. 2001) for calculating the fractions. Also, note that *all* the spectroscopic galaxy members are used to calculate the fractions in each radial bin.

These distributions show that, by taking into account the obscured star formation estimated from the $24\mu\text{m}$ flux, the fraction of star-forming galaxies can dramatically vary at any given radius from the centre of the cluster. In both clusters, the ‘blue’ fraction (f_b) is higher, and flattens at lower cluster-centric radii, than the f_{SF} estimated using the $EW(H_\alpha)$, evidently showing a significant contribution of the post-starburst galaxies to the fraction f_b (also see Section 5.2). We note that this trend may vary if the dusty red galaxies have a non-negligible contribution in building the red se-

quence. But as seen in Fig. 5, in the Coma cluster, this does not seem to be the case.

It is interesting to note that unlike Coma, Abell 1367 has an increasing fraction of blue galaxies with cluster-centric radius (black lines), but an inverse trend emerges when the fractions are measured using the $(24 - z)$ colour (blue lines) or the H_α EW (red lines). This implies that some of the blue galaxies outside the core of Abell 1367 are post-starburst galaxies (see Fig. 12). This result supports the results obtained in the more general work of Mahajan & Raychaudhury (2009), who show that using a single galaxy property, such as the broadband colour, is not an appropriate way of quantifying evolutionary trends like the Butcher-Oemler effect.

5 DISCUSSION

In this paper we set out to understand the relationship between the star formation activity in galaxies, as depicted by an assortment of indicators encompassing the optical and $24\mu\text{m}$ mid-IR wavebands, and their immediate and global environment, in the Coma supercluster. A wide range of local and global environments of galaxies, and a uniform optical coverage across the entire ~ 500 square degrees of sky, make this supercluster an ideal laboratory for examining the environmental dependence of galaxy properties. We discuss below the implications of the results from our analysis presented in §3 and §4.

5.1 The spatial and velocity distribution of galaxies detected at $24\mu\text{m}$

The $24\mu\text{m}$ data for the Coma cluster extend out to a few times its core radius (Fig. 10), allowing us to analyse the spatial (sky and velocity) distribution of the galaxies detected at $24\mu\text{m}$, relative to all the spectroscopic members found in the SDSS. In order to do so, in Fig. 11, we plot the distribution of all the spectroscopic galaxies, and the (optically) red and blue galaxies detected at $24\mu\text{m}$ respectively. As discussed above (Figs. 5 and 6), in Coma both the $24\mu\text{m}$ and optical colours mostly segregate the same galaxies into ‘red’ and ‘blue’ ones. Fig. 11 (top panel) shows that, of the $24\mu\text{m}$ detected galaxies, the distribution of the (optically) red ones is similar to that of all the galaxies, but the (optically) blue ones tend to peak $\gtrsim 1.0 h_{70}^{-1}\text{Mpc}$ from the centre of Coma.

In Fig. 11 (bottom panel), we plot the distribution of the line of sight (l.o.s.) velocities of galaxies, with respect to the mean velocity of the Coma cluster (called the ‘relative velocity’ hereafter), for the same three sets of galaxies. The distribution of the relative velocity of ‘all’ and (optically) red galaxies are statistically similar. But the (optically) blue $24\mu\text{m}$ galaxies show a bimodal distribution, with a large fraction of one mode concentrated around relative velocity $\sim 600 \text{ km s}^{-1}$. A Kolmogorov-Smirnov (K-S) test suggests that the probability of the parent distribution of the relative velocities of red and blue galaxies being sampled from the same population is $p = 8.023 \times 10^{-5}$. The same comparison between the relative velocity distribution of ‘all’ and blue galaxies gives $p = 0.005$, suggesting that it is highly unlikely that the blue and red (or ‘all’) galaxies are drawn from the same parent distribution (Fig. 11). This leads us to conclude that a non-negligible fraction of the (optically) blue $24\mu\text{m}$ galaxies within $2 h_{70}^{-1}\text{Mpc}$ of the centre of the Coma cluster are star-forming galaxies which may belong to the substructure associated with NGC 4839 (see §5.3 for further discussion).

The l.o.s. velocity distribution of the (optically) blue $24\mu\text{m}$

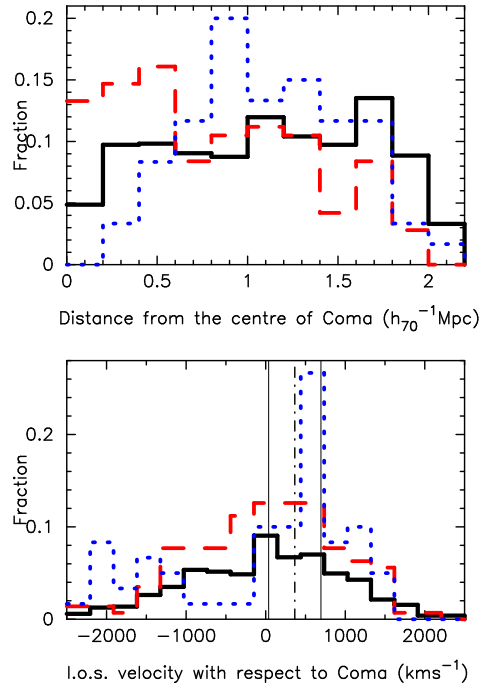


Figure 11. (Top panel): The distribution of cluster-centric distance for all the spectroscopically identified galaxies in a $\pm 3,000 \text{ km s}^{-1}$ slice in the Coma cluster (solid black histogram). The dashed red and dotted blue histograms show the same for the $24\mu\text{m}$ MIPS galaxies, divided into red and blue galaxies on the basis of the $(g-r) - r$ colour-magnitude plot (Figs. 5 & 6). The horizontal axis is limited by the coverage of the MIPS field. Interestingly, even though the red $24\mu\text{m}$ galaxies are uniformly distributed within a $\sim 2 \text{ Mpc}$ radius, the blue galaxy population seems to peak away from the cluster core at $1\text{--}1.5 \text{ Mpc}$ from the centre. **(Bottom panel):** These histograms represent the same galaxies as in the upper panel, but for the l.o.s. velocity of galaxies, relative to the mean redshift of the Coma cluster. Intriguingly, while the red galaxies follow the distribution of all the spectroscopic galaxy members of the Coma cluster, the blue $24\mu\text{m}$ galaxies show a remarkable peak around the velocity of the galaxy group NGC 4839, shown here as the dot-dashed line, with $\pm\sigma_v = 329 \text{ km s}^{-1}$ (Colless & Dunn 1996).

galaxies is highly non-Gaussian, with an excess at $\sim 600 \text{ km s}^{-1}$, suggesting that many of them have recently entered the cluster. If these blue $24\mu\text{m}$ galaxies were virialized, a Gaussian distribution centered on 0, like that seen for the red (red dashed histogram) and ‘all’ (solid black histogram) galaxies would be expected.

The current episode of star formation in these galaxies can be attributed to the environmental impact of the cluster’s ICM (e.g. Poggianti et al. 2004), or the enhanced galaxy density in the infall region (e.g. Mahajan, Raychaudhury & Pimblet 2010). This result is consistent with the findings of Caldwell & Rose (1997), who analysed the spectra of early-type galaxies in 5 nearby clusters, including Coma, and found that in 4 of the 5 clusters, the early-type galaxies show signatures of recent star formation in their spectra (also see §5.2).

5.2 The distribution of k+A galaxies

The post-starburst, or k+A galaxies, as they are popularly known in the literature, are passive galaxies that have recently (1–1.5 Gyr) experienced a strong burst of star formation. These galaxies are very crucial in understanding the impact of environment on various galaxy properties, especially their SFR. The spectrum of a k+A

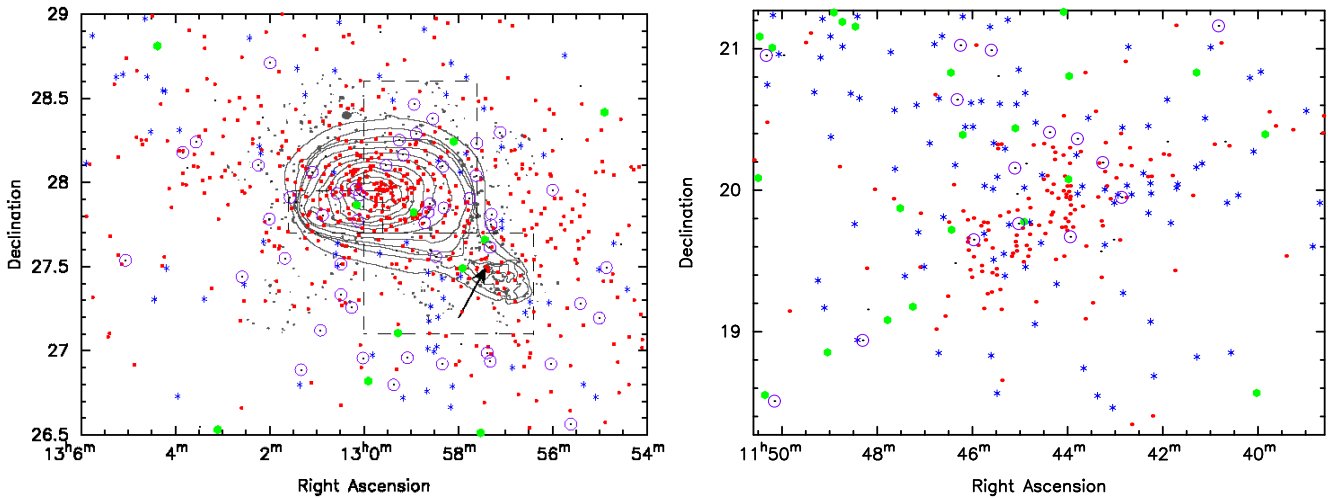


Figure 12. (Left panel): The distribution of the passive (red dots), AGN host (green points), star-forming (blue stars) and the post-starburst (k+A) (purple circles) galaxies in $\sim 5.0 \times 4.2 h_{70}^{-1}$ Mpc region surrounding the centre of Coma. The contours show X-ray emission from a *XMM-Newton* EPIC/PN observation. As can be noticed, not only the star-forming, but also the k+A galaxies seem to avoid the dense cluster centre. Also, the presence of k+A galaxies out to almost twice the virial radius from the centre shows how strong the impact of the ‘global’ cluster environment is on the evolution of galaxies in the vicinity of massive structures. **(Right panel):** Same as above, but for the $5.0 \times 5.0 h_{70}^{-1}$ Mpc region surrounding the centre of Abell 1367. It is interesting to see that in contrast with Coma, most of the k+A galaxies in Abell 1367 seem to be aligned along the direction of the filament feeding it from the direction of Coma. We also note that the (optical) AGN in both the clusters are mostly found in the direction of the filament connecting Coma and Abell 1367.

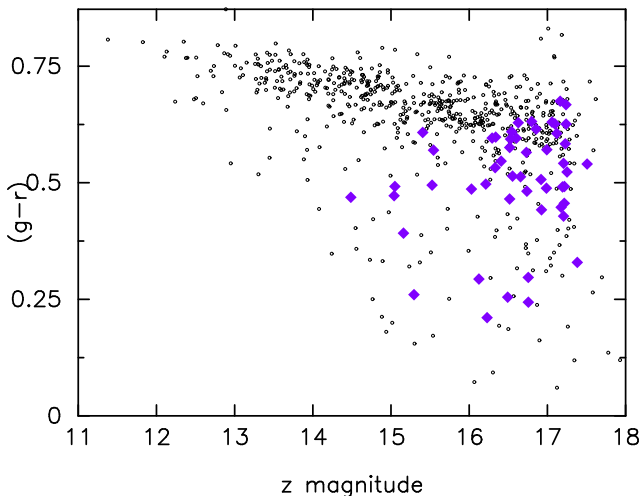


Figure 13. The $(g-r) - z$ colour-magnitude diagram of all the spectroscopically identified galaxies (black points) in the $\sim 5.0 \times 4.2 h_{70}^{-1}$ Mpc region surrounding the centre of the Coma cluster (shown in Fig. 12). The k+A galaxies (purple diamonds) are mostly blue dwarfs. These observations confirm that the low-mass galaxies are the first ones to experience and reflect the impact of rapid change in their local environment.

galaxy shows strong absorption in H_{δ} , but little or no emission in H_{α} .

In this work we make use of the SDSS DR7 spectroscopic galaxy catalogue ($r \leq 17.77$) for identifying the k+A galaxies ($EW(H_{\delta}) < -3\text{\AA}$ & $EW(H_{\alpha}) < 2\text{\AA}$) in the Coma supercluster (Please note that throughout this work, negative values of EW indicate absorption). In Fig. 12 we show these k+A galaxies together with the passive, star-forming and AGN galaxies in and around the Coma and Abell 1367 cluster respectively. As can be easily seen, the k+A galaxies preferentially avoid the dense region in the cluster core but inhabit the surrounding infall regions out to $\sim 5 h_{70}^{-1}$ Mpc (almost twice the virial radius). In Fig. 12 we have also over-plotted

the contours of intensity from the mosaicked 0.5–2 keV image of the core of Coma cluster from *XMM-Newton* EPIC/PN observations (Finoguenov, Briel, & Henry 2003), kindly supplied to us by A. Finoguenov. We note that there are almost no star-forming galaxies in the X-ray emitting region of the core. This observation further strengthens the argument that the changes in environment, experienced by a galaxy on the outskirts of clusters, play a key role in modulating the properties of galaxies, especially the dwarfs (e.g. Porter et al. 2007, 2008).

By analysing deep ($M_B \lesssim -14$) photometric and spectroscopic optical data for 3 regions in Coma (two near the centre and one near NGC 4839, each $\sim 1 \times 1.5$ Mpc in size), Poggianti et al. (2004) found that $\sim 10\%$ of the cluster’s dwarf ($M_V > -18.5$) galaxies have post-starburst spectra. They also used the results from the X-ray analysis of Neumann et al. (2003) to show that the k+A galaxies in the Coma cluster are likely to be a result of the interaction between the Coma cluster and the adjoining NGC 4839 galaxy group (see §5.3). In Fig. 12, we overplot as dashed rectangles, the approximate location of the substructures found by Neumann et al. (2003). As has been shown by Poggianti et al. (2004, their fig. 6), on the western side of the Coma cluster, the k+A galaxies seem to lie along the X-ray substructure (also see fig. 2 of Neumann et al. 2003). We demonstrate this by overplotting contours of X-ray intensity in Fig. 12.

However, it is also interesting to note that the southern substructure, apparent from the X-ray contours, is almost devoid of k+A galaxies, but has a stream of star-forming dwarf galaxies flowing towards the cluster core (Fig. 4; also see §5.4). Contrary to Poggianti et al. (2004), by taking into account the extended region surrounding the Coma cluster, we find that the k+A galaxies preferentially avoid the cluster core but their spatial distribution does not show any correlation with the substructure evident in the X-ray emission (Fig. 12).

In Fig. 13 we examine the position of the k+A galaxies in the Coma cluster in the plot of $(g-r)$ colour vs z magnitude. Fig. 13 show that almost all the k+A galaxies in Coma are dwarfs

Table 2. Dwarf ($z > 15$ mag) galaxies in the Coma supercluster

	Total	Star-forming	k+A
Coma ($\sim 5 \times 4.2 \text{ Mpc}^2$; Fig. 12)	438	55	50
Abell 1367 ($\sim 5 \times 5 \text{ Mpc}^2$; Fig. 12)	391	203	19
Supercluster (excluding regions mentioned above)	1106	667	23

($z \lesssim 15$), suggesting that either only the infalling dwarf galaxies are rapidly quenched, or the SFR- M^* relation (e.g. Feulner et al. 2005) dilutes the post-starburst signature in massive galaxies. Since dwarf k+A galaxies in the Coma supercluster are found on the outskirts of Coma and Abell 1367 clusters, and occasionally in galaxy groups embedded elsewhere in the large-scale structure (LSS), this might suggest that dwarf galaxies falling into deeper potentials are more likely to show k+A features, while those being assimilated into galaxy groups may be quenched on a longer time-scale. We will probe this in greater detail in a later paper.

The handful of galaxies with very blue colours ($(g-r) < 0.5$; Fig. 13) are the k+A dwarfs in which the episode of starburst could have ended ~ 300 Myr ago, unlike the more evolved red post-starburst dwarfs (Poggianti et al. 2004). By studying spectra of early-type galaxies ($M_b < 16.7$) in Coma, Caldwell & Rose (1997) also found that $\sim 15\%$ of these galaxies show signatures of recent or ongoing star formation. Based on this result, Caldwell & Rose (1997) suggested that the present day clusters act as a catalyst for galaxy evolution, though at a reduced level as compared to their high redshift counterparts.

Given the vulnerable nature of dwarf galaxies, it is not surprising that a large fraction of them are the first ones to reflect the impact of rapid changes in their environment during the transition from filament to cluster. This contributes to dwarf galaxies having a better-defined SF-density relation, relative to their more massive counterparts (Fig. 4). Table 2 shows that 11.4% of dwarfs in Coma, 4.8% in Abell 1367 and 2.1% in the neighbouring supercluster region have spectra with k+A features. This evidently shows that the mechanisms responsible for quenching star formation in dwarf galaxies and rapidly transforming them to passive galaxies via the post-starburst phase, are strongly dependent on the cluster potential. This result is also in agreement with the observation of excessive red, dwarf ellipticals (dEs) in the Coma cluster (Jenkins et al. 2007). In Table 3 we provide a list of all the 110 k+A dwarf ($z > 15$) galaxies found in the entire Coma supercluster.

5.3 Coma and NGC 4839

As noted above, the Coma cluster is known to have significant substructure in the optical and X-ray maps. The most prominent X-ray emitting substructure is associated with a galaxy group, of which NGC 4839 is the most prominent galaxy. By combining N-body hydrodynamical simulations with *ROSAT* X-ray and VLA radio observations, Burns et al. (1994) remarked that the NGC 4839 group has already passed through the core of Coma ~ 2 Gyr ago, and is now on its second infall (also see Caldwell & Rose 1997). However, several other studies based on optical spectroscopy and imaging, and X-ray observations conclude otherwise (Colless & Dunn 1996; Neumann et al. 2003; Adami et al. 2005). No consensus seems to have been reached on the dynamical state of NGC 4839. Studies supporting the first infall argument suggest

Table 3. Catalogue of dwarf ($z > 15$), k+A ($\text{EW}(\text{H}\alpha) < 2 \text{ \AA}$ & $\text{EW}(\text{H}\delta) < -3 \text{ \AA}$) galaxies in the Coma supercluster (this table is available in full on-line).

RA (J2000)	Dec (J2000)	Redshift	z mag	$\text{EW}(\text{H}\alpha)$ \AA	$\text{EW}(\text{H}\delta)$ \AA
195.4972	28.7095	0.0203	16.8559	-1.9535	-20.5023
194.7338	28.4636	0.0198	15.1591	-2.6499	-5.6373
174.6209	28.5871	0.0236	15.3615	1.8792	-3.9275
192.4220	28.8448	0.0218	17.1838	-1.3320	-30.0913
192.8569	28.7203	0.0241	17.0417	-1.1904	-3.1975
193.9028	26.5644	0.0211	16.9923	-1.8170	-6.2012
194.5201	26.3706	0.0232	15.7774	-1.8387	-6.3831
195.0435	26.4612	0.0221	16.6272	-2.0973	-3.2747
189.0882	27.0333	0.0251	16.6488	-1.9006	-3.0789
194.0083	26.9208	0.0191	16.5278	-1.4534	-4.9134

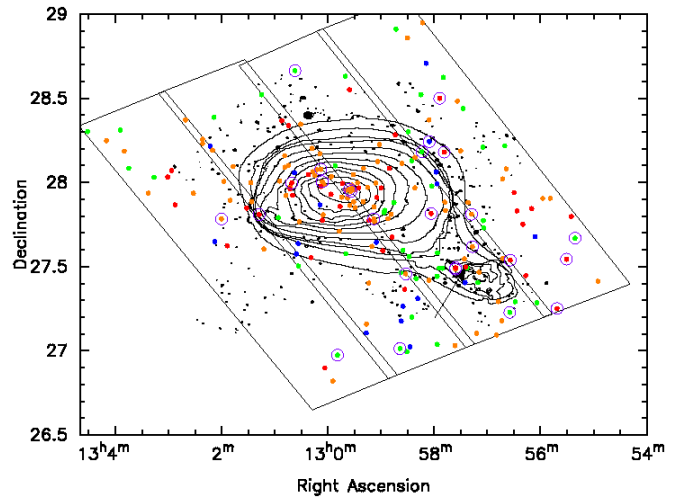


Figure 14. The spatial distribution of galaxies detected at $24\mu\text{m}$ in the Coma Supercluster region. The galaxies are coded by their $(24-z)$ colour as following: red: > -4 , orange: $-4 \leq (24-z) < -6$, green: $-6 \leq (24-z) < -8$ and blue: ≤ -8 . The purple circles are the blue $24\mu\text{m}$ galaxies moving at velocities similar to that of the NGC 4839 galaxy group (i.e. having l.o.s. velocity = $7339 \pm 329 \text{ km s}^{-1}$; Colless & Dunn 1996). We note that 19 of these 26 galaxies have $(24-z)$ colour corresponding to that of the passive galaxies (i.e. $(24-z) \leq -6$; Fig. 6). The contours are from a 0.5–2 keV XMM-Newton EPIC/PN X-ray mosaic image of the extended Coma cluster.

that the NGC 4839 galaxy group has a velocity dispersion (σ_{cz}) of 329 km s^{-1} (e.g. Colless & Dunn 1996), while others claim it to be as high as 963 km s^{-1} (e.g. Caldwell et al. 1993), the latter being consistent with the scenario where the galaxies belonging to the group have dispersed during their first passage through the cluster.

Located ~ 1.1 Mpc from the centre of the Coma cluster, the NGC 4839 galaxy group was first detected as an asymmetric extension to the otherwise relaxed X-ray morphology of Coma (Briel, Henry and Böhringer 1992). Several authors have discovered post-starburst (k+A) galaxies associated with this group (Caldwell et al. 1993; Caldwell & Rose 1997; Poggianti et al. 2004). In this work, we find that most of the known post-starburst galaxies in Coma, such as those found by Poggianti et al. (2004), are either not detected at $24\mu\text{m}$, or show little MIR emission. We hence confirm that almost none of these post-starburst galaxies have a significant amount of obscured star formation going on in them.

Struck (2006) suggests that when a galaxy group passes through the core of a cluster, as suggested by Burns et al. (1994) for Coma and NGC 4839, the group galaxies are gravitationally shocked. In this scenario, enhancement in star formation activity is a natural consequence of an increase in galaxy-galaxy interactions among group galaxies. Such a scenario has been suggested for Coma and NGC 4839 by Neumann et al. (2003). Fig. 14 may provide circumstantial evidence to support this argument.

In Fig. 14 we show the spatial distribution of the $24\mu\text{m}$ detected Coma galaxies colour-coded by their $(24-z)$ colour. The blue $24\mu\text{m}$ galaxies constituting the peak, which also corresponds to the mean velocity of the NGC 4839 group (Fig. 11), are explicitly shown. However, poor statistics in our data do not allow us to favour any of the 2 scenarios associated with the NGC 4839 galaxy group and the Coma cluster, namely, (i) whether the group is on its first infall, or (ii) it has already passed through the core and is on its second passage.

5.4 Coma, Abell 1367 and the filament

In the hierarchical model, galaxy clusters grow by accretion and/or mergers with other clusters and groups. In simulations, galaxies are seen to be accreted along the network of filaments of galaxies, feeding these clusters, along preferred directions (e.g. Bond, Kofman, & Pogosyan 1996). Although several observational techniques are now being implemented to detect and quantify such large-scale structures (LSS), the low surface density of matter, enormous spatial scale, and projection effects make it difficult to observe the extent of these filaments of galaxies (Colberg 2007).

One way of exploring the evolution of the LSS is to probe its impact on the galaxies traversing them. The spectacular filament crossing the Coma and Abell 1367 clusters is an exclusive object in the low redshift Universe, because it is not only traced by the spatial distribution of galaxies (Fig. 1), but has also been detected at radio wavelengths (Kim et al. 1989). One of the aims of this paper is to understand and interpret the difference in the evolutionary paths adopted by galaxies in the vicinity of the clusters, the filament and the groups embedded in the filament. In agreement with the scenario emerging in the literature (Gray et al. 2004; Tanaka et al. 2004; Smith et al. 2006; Haines et al. 2007, among others), we find that the SFR-density relation across the Coma supercluster is much weaker for the massive galaxies ($z < 14.5$; Fig. 3), relative to the dwarfs ($z > 15$; Figs. 3 & 4).

Empirical studies of galaxies infalling into clusters along filaments suggest that an enhanced galaxy density at the cluster periphery may lead to a burst of star formation in them, consuming a large fraction of cold gas (e.g. Porter et al. 2008; Mahajan, Raychaudhury & Pimblet 2010). This effect would be more efficient for the dwarf galaxies. In a study based on the SDSS data, Haines et al. (2007) find that the dwarf galaxies ($-19 < M_r < -18$) residing in high density regions show a systematic reduction of $\sim 30\%$ in their H_α emission relative to the mean of the sample, leading the authors to favour slow quenching of star formation in these galaxies (also see Balogh et al. 2004a; Tanaka et al. 2004). On the contrary, in Coma we find that the infalling star-forming dwarf galaxies undergo a burst of star formation, followed by rapid quenching (Fig. 4, also see Section 5.2).

In contrast, star formation in dwarf galaxies infalling into galaxy groups, seems to be slowly quenched without an intermediate starburst phase, resulting in the observed reduction in the mean $\text{EW}(H_\alpha)$ values seen in the vicinity of groups in Fig. 4. This observation could be attributed to the relatively inefficient ram-pressure

stripping in galaxy groups (Tanaka et al. 2004), transforming infalling galaxies slowly over several Gyr via a process involving progressive starvation (Larson, Tinsley & Caldwell 1980).

Another notable fact in Fig. 4 is the orientation of the stream of blue star-forming galaxies southward of Coma, almost orthogonal to the direction of elongation of the galaxy density (Figs. 3 & 4). This may be significant given the observations presented in the previous section (also see Burns et al. 1994). Consistent with the results presented in literature, we find that the instantaneous SFR of a galaxy depends upon the stellar mass of the galaxy, as well as on the local galaxy density, and on whether the galaxy is in a group or cluster. The cosmic web does play a crucial role in defining the evolutionary path of the galaxy, as is seen by different rate of quenching of dwarf galaxies in groups and clusters (Fig. 4). The different fractions of dwarf k+A galaxies in the three major components of this supercluster further strengthens this argument (Table 2). It is indeed remarkable that the Coma and Abell 1367 clusters, that are well known to have very different galaxy properties, influence the star formation histories of the infalling galaxies very differently. While the fraction of star-forming and k+A dwarf galaxies in Abell 1367 vary by a factor of 10 ($\sim 52\%$ & 4.8% respectively; Table 2), in the Coma cluster neither dominate (12.5% & 11.4% respectively; Table 2).

6 CONCLUSIONS

This work is a step ahead in understanding the star formation properties of galaxies in one of the richest nearby superclusters. We analyse the spectroscopic and photometric data obtained by the SDSS and archival $24\mu\text{m}$ data obtained by the MIPS instrument on board *Spitzer*. Our major results are:

- The fraction of (optical) AGN drops significantly ($f_{AGN} < 0.25$) in the dense cluster environment. But the relation between AGN activity and environment is unclear in the intermediate density environments of galaxy groups.
- Star formation in massive galaxies ($z < 14.5$) seems to be low everywhere in the supercluster region studied here, almost independent of the local environment. In sharp contrast, the dwarf galaxies ($z > 15$) can be seen to be rapidly forming stars everywhere, except in the dense cluster and group environments.
- The passive, AGN host and star-forming galaxies as classified from their optical spectra, occupy different regions on the $(24-z)-(g-r)$ colour-colour diagram.
- The fraction of star-forming galaxies in Coma is determined to within $\pm 10\%$, irrespectively of the definition of star-forming in terms of optical $(g-r)$ colour, optical-mid-IR $(24-z)$ colour or $\text{EW}(H_\alpha)$. Many of the blue galaxies in Coma are found to be post-starburst galaxies, whose blue colours are due to a recent burst of star formation which has now terminated, as revealed by their lack of H_α emission and excess H_δ absorption. However, in Abell 1367, the f_{SF} obtained using the 3 different indicators show different trends. While the fraction of blue galaxies increases outward from the centre, the f_{SF} obtained by employing the $(24-z)$ near/mid IR colour decreases away from the centre of Abell 1367.
- Most of the (optically) blue $24\mu\text{m}$ galaxies detected in Coma are on their first infall towards the cluster. The current episode of star formation in such galaxies is possibly a result of a rapidly changing local environment.
- 11.4% of all dwarf ($z > 15$) galaxies within $5 \times 4.2 h_{70}^{-1} \text{Mpc}^2$ of the centre of Coma, and 4.8% within the same area around

Abell 1367 have post-starburst (k+A) type spectra. In the surrounding supercluster region this fraction drops to 2.1% only, suggesting that the mechanism(s) responsible for quenching star formation in dwarfs depends upon the cluster's potential. The starburst, rapid quenching and subsequent k+A phase requires the dense ICM and high infall velocities attainable in rich clusters, as opposed to galaxy groups where star formation in infalling dwarf galaxies appears to be quenched gradually. The k+A galaxies preferentially avoid the dense centre of the cluster.

- The spatial distribution of the k+A galaxies suggests a correlation between the substructure of the Coma cluster (revealed in the X-ray emission) and the mechanisms responsible for quenching star formation in galaxies.

7 ACKNOWLEDGMENTS

We thank Dr Alexis Finoguenov and Dr Ulrich Briel for providing us the XMM-Newton EPIC/PN 0.5–2 keV mosaic image of the Coma cluster used in Figs. 12 and 14. SM is supported by grants from ORSAS, UK, and the University of Birmingham. CPH acknowledges financial support from STFC. We are very grateful to the anonymous referee for constructive comments that were very helpful in improving this paper.

This research has made use of the SAO/NASA Astrophysics Data System, and the NASA/IPAC Extragalactic Database (NED). Funding for the SDSS and SDSS-II has been provided by the Alfred P. Sloan Foundation, the Participating Institutions, the National Science Foundation, the U.S. Department of Energy, the National Aeronautics and Space Administration, the Japanese Monbukagakusho, the Max Planck Society, and the Higher Education Funding Council for England. A list of participating institutions can be obtained from the SDSS Web Site <http://www.sdss.org/>.

REFERENCES

- Adami C., Biviano A., Durret F., Mazure A., 2005, *A&A*, 443, 17
 Adelman-McCarthy et al., J. K., 2006, *ApJS*, 162, 38
 Arnold T. J., Martini P., Mulchaey J. S., Berti A., Jeltema T. E., 2009, arXiv, arXiv:0911.0392
 Bai L., Rieke G. H., Rieke M. J., Hinz J. L., Kelly D. M., Blaylock M., 2006, *ApJ*, 639, 827
 Bai, L., Rasmussen, J., Mulchaey, J. S., Dariush, A., Raychaudhury, S., Ponman, T. J., 2010, *ApJ*, submitted
 Baldwin J. A., Phillips M. M., Terlevich R., 1981, *PASP*, 93, 5
 Balogh M. L., Navarro J. F., Morris S. L., 2000, *ApJ*, 540, 113
 Balogh M., et al., 2004, *MNRAS*, 348, 1355
 Balogh M. L., Navarro J. F., Morris S. L., 2000, *ApJ*, 540, 113
 Bell E. F., McIntosh D. H., Katz N., Weinberg M. D., 2003, *ApJS*, 149, 289
 Bernstein G. M., Guhathakurta P., Raychaudhury S., Giovanelli R., Haynes M. P., Herter T., Vogt N. P., 1994, *AJ*, 107, 1962
 Berrier J. C., Stewart K. R., Bullock J. S., Purcell C. W., Barton E. J., Wechsler R. H., 2009, *ApJ*, 690, 1292
 Bertin E., Arnouts S., *A&AS*, 117, 393
 Best, P. N., Kauffmann, G., Heckman, T. M., Brinchmann, J., Charlot, S., Ivezić, Ž., & White, S. D. M. 2005, *MNRAS*, 362, 25
 Bildfell C., Hoekstra H., Babul A., Mahdavi A., 2008, *MNRAS*, 389, 1637
 Blanton M. R., et al., 2001, *AJ*, 121, 2358
 Blanton M. R., Eisenstein D., Hogg D. W., Zehavi I., 2006, *ApJ*, 645, 977
 Bond J. R., Kofman L., Pogosyan D., 1996, *Nature*, 380, 603
 Boselli A., Gavazzi G., Lequeux J., Buat V., Casoli F., Dickey J., Donas J., 1997, *A&A*, 327, 522
 Boselli A., et al., 1997, *A&A*, 324, L13
 Bothun G. D., Schommer R. A., Sullivan W. T., III, 1984, *AJ*, 89, 466
 Bressan A., et al., 2006, *ApJ*, 639, L55
 Briel U. G., Henry J. P., Böhringer H., 1992, *A&A*, 259, L31
 Burns J. O., Roettiger K., Ledlow M., Klypin A., 1994, *ApJ*, 427, L87
 Butcher H., Oemler A., Jr., 1984, *ApJ*, 285, 426
 Caldwell N., Rose J. A., Sharples R. M., Ellis R. S., Bower R. G., 1993, *AJ*, 106, 473
 Caldwell N., Rose J. A., 1997, *AJ*, 113, 492
 Calzetti D., et al., 2005, *ApJ*, 633, 871
 Calzetti D., et al., 2007, *ApJ*, 666, 870
 Chincarini G., Rood H. J., 1976, *ApJ*, 206, 30
 Clemens M. S., Bressan A., Panuzzo P., Rampazzo R., Silva L., Buson L., Granato G. L., 2009, *MNRAS*, 392, 982
 Colberg J. M., 2007, *MNRAS*, 375, 337
 Colless M., Dunn A. M., 1996, *ApJ*, 458, 435
 Cortese L., Gavazzi G., Boselli A., Iglesias-Páramo J., Carrasco L., 2004, *A&A*, 425, 429
 Cortese L., Gavazzi G., Boselli A., 2008, *MNRAS*, 390, 1282
 Davis D. S., Mushotzky R. F., 1993, *AJ*, 105, 409
 Del Pozzo W., Raychaudhury S., Babul A., 2010, submitted to *MNRAS*
 De Propriis R., et al., *MNRAS*, 2004, 351, 125
 Dressler A., 1980, *ApJS*, 42, 565
 Dressler A., Shectman S. A., 1988, *AJ*, 95, 985
 Ellingson E., Lin H., Yee H. K. C., Carlberg R. G., 2001, *ApJ*, 547, 609
 Feulner G., Goranova Y., Drory N., Hopp U., Bender R., 2005, *MNRAS*, 358, L1
 Finoguenov A., Briel U. G., Henry J. P., 2003, *A&A*, 410, 777
 Fontanelli P., 1984, *A&A*, 138, 85
 Goulding A. D., Alexander D. M., 2009, *MNRAS*, 398, 1165
 Geller M. J., Huchra J. P., 1989, *Sci*, 246, 897
 Giovanelli R., Haynes M. P., 1985, *ApJ*, 292, 404
 Gray M. E., Wolf C., Meisenheimer K., Taylor A., Dye S., Borch A., Kleinheinrich M., 2004, *MNRAS*, 347, L73
 Gregory S. A., Thompson L. A., 1978, *ApJ*, 222, 784
 Haines C. P., Merluzzi P., Mercurio A., Gargiulo A., Krusanova N., Busarello G., La Barbera F., Capaccioli M., 2006, *MNRAS*, 371, 55
 Haines C. P., Gargiulo A., La Barbera F., Mercurio A., Merluzzi P., Busarello G., 2007, *MNRAS*, 381, 7
 Haines C. P., Gargiulo A., Merluzzi P., 2008, *MNRAS*, 385, 1201
 Haines C. P., et al., 2009, *ApJ*, 704, 126
 Hickox R. C., et al., 2009, *ApJ*, 696, 891
 Iglesias-Páramo J., Boselli A., Gavazzi G., Cortese L., Vílchez J. M., 2003, *A&A*, 397, 421
 Jenkins L. P., Hornschemeier A. E., Mobasher B., Alexander D. M., Bauer F. E., 2007, *ApJ*, 666, 846
 Kauffmann G., White S. D. M., Heckman T. M., Ménard B., Brinchmann J., Charlot S., Tremonti C., Brinkmann J., 2004, *MNRAS*, 353, 713
 Kennicutt R. C., et al., 2009, *ApJ*, 703, 1672
 Kim K.-T., Kronberg P. P., Giovannini G., Venturi T., 1989, *Nature*, 341, 720

- Knapp G. R., Guhathakurta P., Kim D., Jura M. A., 1989, *ApJS*, 70, 329
- Larson R. B., Tinsley B. M., Caldwell C. N., 1980, *ApJ*, 237, 692
- Lee J. C., Kennicutt R. C., José G. Funes S. J., Sakai S., Akiyama S., 2009, *ApJ*, 692, 1305
- Le Floch E., et al., 2005, *ApJ*, 632, 169
- Leitherer C., et al., 1999, *ApJS*, 123, 3
- Mac Low M.-M., Ferrara A., 1999, *ApJ*, 513, 142
- Mahajan S., Raychaudhury S., 2009, *MNRAS*, 400, 687
- Mahajan S., Raychaudhury S., Pimblet K. A., 2010, in preparation
- Marcolini A., D'Ercole A., Brighenti F., Recchi S., 2006, *MNRAS*, 371, 643
- Margoniner V. E., de Carvalho R. R., 2000, *AJ*, 119, 1562
- Martini P., Kelson D. D., Kim E., Mulchaey J. S., Athey A. A., 2006, *ApJ*, 644, 116
- Miller C. J., Nichol R. C., Gómez P. L., Hopkins A. M., Bernardi M., 2003, *ApJ*, 597, 142
- Neumann D. M., et al., 2003, *A&A*, 406, 789
- Piovan L., Tantaló R., Chiosi C., 2003, *A&A*, 408, 559
- Pisani A., 1993, *MNRAS*, 265, 706
- Poggianti B. M., Bridges T. J., Komiyama Y., Yagi M., Carter D., Mobasher B., Okamura S., Kashikawa N., 2004, *ApJ*, 601, 197
- Porter S. C., Raychaudhury S., 2007, *MNRAS*, 375, 1409
- Porter S. C., Raychaudhury S., Pimblet K. A., Drinkwater M. J., 2008, *MNRAS*, 388, 1152
- Raychaudhury S., von Braun K., Bernstein G. M., Guhathakurta P., 1997, *AJ*, 113, 2046
- Rieke G. H., et al., 2004, *ApJS*, 154, 25
- Rieke G. H., Alonso-Herrero A., Weiner B. J., Pérez-González P. G., Blaylock M., Donley J. L., Marcillac D., 2009, *ApJ*, 692, 556
- Rines K., Geller M. J., Kurtz M. J., Diaferio A., 2003, *AJ*, 126, 2152
- Saintonge A., Tran K.-V. H., Holden B. P., 2008, *ApJ*, 685, L113
- Shen Y., Mulchaey J. S., Raychaudhury S., Rasmussen J., Ponman T. J., 2007, *ApJ*, 654, L115
- Shupe D. L., et al., 2008, *AJ*, 135, 1050
- Silverman B. W., 1986, *Density Estimation for Statistics and Data Analysis*, Chapman and Hall, London
- Struck C., 2006, *asup.book*, 115
- Smith R. J., Hudson M. J., Lucey J. R., Nelan J. E., Wegner G. A., 2006, *MNRAS*, 369, 1419
- Smith R. J., et al., 2008, *MNRAS*, 386, L96
- Sullivan W. T., III, Johnson P. E., 1978, *ApJ*, 225, 751
- Tanaka M., Goto T., Okamura S., Shimasaku K., Brinkmann J., 2004, *AJ*, 128, 2677
- West M. J., 1998, *ucb.proc*, 36
- Wolf C., et al., 2009, *MNRAS*, 393, 1302
- Yang X., Mo H. J., van den Bosch F. C., Weinmann S. M., Li C., Jing Y. P., 2005, *MNRAS*, 362, 711
- Zheng X. Z., Bell E. F., Papovich C., Wolf C., Meisenheimer K., Rix H.-W., Rieke G. H., Somerville R., 2007, *ApJ*, 661, L41